Separation of dense colloidal suspensions in narrow channels: A stochastic model

Yosyp A. Humenyuk,[1,2] Miroslav Kotrla,[1] Karel Netočný,[1] and František Slanina[1,*]
[1]*Institute of Physics, Czech Academy of Sciences, Na Slovance 2, CZ-18221 Praha, Czech Republic*
[2]*Institute for Condensed Matter Physics of the National Academy of Sciences of Ukraine, 1 Svientsitskii St, UA-79011 Lviv, Ukraine*

(Received 29 November 2019; accepted 6 March 2020; published 24 March 2020)

The flow of a colloidal suspension in a narrow channel of periodically varying width is described by the one-dimensional generalized asymmetric exclusion process. Each site admits multiple particle occupancy. We consider particles of two different sizes. The sites available to particles form a comblike geometry: entropic traps due to variation of channel width are modeled by dead ends, or pockets, attached individually to each site of a one-dimensional chain. This geometry, combined with periodically alternating external driving, leads to a ratchet effect which is very sensitive to particle size, thus enabling particle sorting. A typical behavior is reversal of the current orientation when we change the density of small and big particles. In an optimal situation, the two types of particles move in opposite directions, and particle separation is in principle perfect. We show that in the simplest situation with one type of particles only, this model is exactly soluble. In the general case we use enhanced mean-field approximation as well as direct numerical simulations.

DOI: 10.1103/PhysRevE.101.032608

I. INTRODUCTION

The problem of movement of driven and strongly interacting classical particles in confined geometries occurs very often in numerous applications [1,2]. One of the first motivations for study of these systems occurred in molecular biology [3,4]. When synthesizing proteins, ribosomes slide along the RNA chain, driven by a molecular motor. There are many ribosomes attached one after the other on the same RNA chain, and as they are not synchronized, they interact strongly by steric repulsion. The situation can be described in terms of the asymmetric exclusion process (ASEP) [5]. This model, due to its conceptual simplicity, became very popular during the last decades. It is exactly solvable either using the Bethe ansatz or using the matrix product technique [6–14]. It was found that it is a paradigmatic model for a very wide range of situations sharing the same dynamic universality class [15,16].

The success and popularity of the ASEP stimulated its use for more realistic situations. We already mentioned the early application to ribosome movement. Ribosomes are just one of many examples of molecular motors at work in living cells [17–20]. The molecular motors rely on the mechanism of a Brownian ratchet [21], i.e., on periodic alteration of the effective potential in which the motor particle moves. Such alteration is spatially indiscriminate, nevertheless it produces driven motion in a specific direction. Experiments show various complex phenomena which manifest strong interactions between molecular motors [22–26]. To model them, the ASEP was often combined with the ratchet mechanism, as a starting point to develop more complicated models with internal degrees of freedom and complex dynamics [27–39].

The typical length scale of molecular motors is about 10 nm. On a much larger scale, about 1 μm and more, similar physics is observed in dense suspensions of colloidal particles in narrow pores or various microfluidic chambers [1,40–43]. Driving is provided by the flow of surrounding liquid only, or combining it with gravity, electrostatic field, centrifugation, etc. One of the important tasks we face in such systems is separation of colloidal particles according to their size, shape, or other physical properties [44–46]. Among numerous applications, let us mention, for example, separation of alien particles from blood [47–49]. As a pedagogical example, blood is perhaps the most illuminating case. Indeed, there are numerous, but not extremely many, types of blood cells, all of them at a scale about 10 μm, and they form a rather dense suspension driven by blood pressure. Contact interaction between cells is strong due to considerable density, and driving is also strong in order to keep them in movement. If there are alien cells in very small concentration, e.g., originating from a tumor, it is delicate task to find them among all the rest. Physical methods, like inertial migration [50], have the invaluable advantage of being nondestructive; therefore, the captured cells may be further analyzed, cultivated, etc. Another strategy based on hydrodynamics is provided by deterministic lateral displacement where particles pass through a two-dimensional array of obstacles [51,52]. Diffusion-driven sorting in such two-dimensional structures was studied in Refs. [53,54].

In our work, we focus on separation of particles in channels and tubes of various asymmetric geometric structure. The most typical shape is the "sawtooth" profile, where the width of the channel periodically increases and decreases. The behavior of colloidal suspensions in such channels was widely studied experimentally [55–59], confirming the separation capacity of these devices. Theoretical modeling of these systems was done mostly in the low-density regime, where particles are nearly independent [60–62], but simulations are also available for dense suspensions of hard spheres [63] or

*slanina@fzu.cz

Lennard-Jones particles [64]. The clue to separation mechanism lies in the ratchet mechanism, as explained above. It was shown that the key ingredient of such channels as separating devices comes from the wider areas of the channel. They act as weak or strong traps (depending on the shape) where particles may be kept off the current of other particles. In specific geometries, such traps, or pockets, may even lead to negative mobility of the particles [65–67].

The idea of our work comes from combination of the channel geometry containing arrays of pockets with the idealized dynamics provided by the ASEP model. The fact that there are several species of particles, which can differ in their mobility, size, etc., will require some generalization of the ASEP model. However, we shall still profit from its conceptual simplicity and the ease of implementation in simulations.

In fact, the ASEP with several species of particles was studied quite in depth [68–77]. As long as the exclusion property is kept, i.e., if there is at most one particle at a site, the multispecies ASEP remains to be integrable, and many properties are known exactly. The situation changes if we allow more particles per site [78]. This family of models is commonly called generalized exclusion process (GEP). The situation is much simpler in symmetric case, where unidirectional driving is absent. Numerous results are known for symmetric GEP [79–83], and although it does not seem to be integrable, except for special cases (e.g., the misantrope process [84]), approximative methods yield surprisingly precise results when compared with numerical simulations [80].

For our purposes, we need to include asymmetric driving, so the asymmetric GEP, or the generalized ASEP, will be used [85]. Here we further generalize this model by allowing two species of particles. These two species will model the situation of a dense colloidal mixture, whose components need to be separated. This situation was already modeled in terms of a two-lane ASEP [86–88], where interaction between lanes partially accounts for two particles being at the same site. A similar two-lane perspective was also applied in Ref. [89], while in Ref. [90] particles could have different length, i.e., they can occupy different number of adjacent sites. Also in our model the particles will have a different size, but we shall require that one particle can occupy at most one site. The sum of the sizes of all particles at the same site cannot exceed a fixed number we shall call site capacity.

Second generalization introduced here will affect the geometry of the structure on which the particles move. In order to mimic the channels of variable width, we abandon the strict linear chain of sites. In earlier models each site was a cell within which particles were placed. In our model, each site is an object composed of two cells. The linear chain of cells serves as a kind of a backbone and to each cell on the backbone we append another cell as a dead end or a pocket. The pockets are isolated from each other, so the particles can jump just from the backbone to a pocket and back. This way, particles diffuse on a kind of an asymmetric comblike structure. Such structure is crucial for the emergence of the ratchet effect, i.e., rectification of the net particle current, when the direction of the external driving is periodically alternated. Indeed, in the original ASEP and all its generalizations keeping the linear chain geometry, the current just changes sign when the direction of driving is altered, resulting in zero ratchet current. The nonzero ratchet current can occur only due to the presence of pockets.

In the Sec. II we define our generalized ASEP model, show an exactly solvable case, and specify in detail the Monte Carlo simulations used. Comparison with these simulations is made throughout the following sections. In Sec. III we start with mean-field approximation in methodologically useful simplified cases. In Sec. IV we solve the full generalized ASEP model using the mean-field approximation and discuss the agreement with Monte Carlo simulations. In Sec. V we investigate the ratchet effect and its use for full separation of particles according to their size. Section VI summarizes the results obtained.

II. GENERALIZED ASEP MODEL

A. Discretized and stochastic description

We want to model a dense suspension of colloid particles moving in a pore with nontrivial geometry. The particles are suspended in a fluid, but we assume they are neutrally buoyant. The particles are driven by an external bias, due to either a hydrodynamic drift or an external field. They interact with each other and with the walls of the pore by steric repulsion. Hydrodynamic interactions due to surrounding fluid are neglected. We say in advance that such neglect is a serious weak point of our approach, because in reality the hydrodynamic interactions, especially with the walls, are quite strong. On the other hand, it greatly simplifies the treatment, as the principal factors of the movement are drift and diffusion. These two factors can be then effectively accounted for by stochastic modeling.

The first ingredient of our model will be the simplified geometry of the pore in which the particles move. We suppose the diameter of the pore varies periodically along its axis. Inside the pore, a mixture of particles of various sizes is moving. We show the situation schematically in Fig. 1(a).

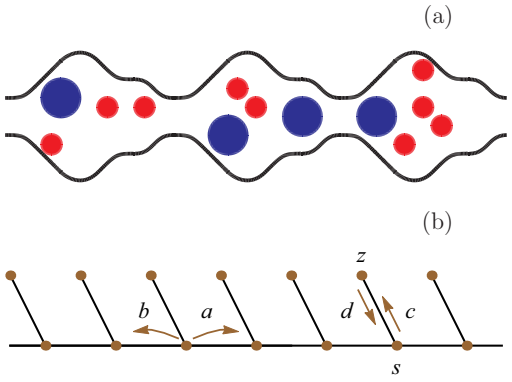

FIG. 1. (a) Schematic picture of a pore with periodically varying diameter, containing a mixture of colloidal particles. Note that the variation is mirror-asymmetric. (b) Model idealization of such pore, featuring an asymmetric comblike structure of cells. The structure consists of a backbone with attached dead ends, or pockets. These pockets represent locations where the diameter of the pore is increased. The jump rates along the links connecting the cells are indicated by quantities a, b, c, and d.

In view of ASEP-like modeling, we mimic such a pore geometry by a discretized version. Instead of having continuous values for the positions of the particles we divide the space available into cells, and for each particle we register only the presence or absence of the particle in certain cell, not the precise position within the cell. In order to measure the size of the cell, we introduce the cell capacity k. As our primary concern is separation of mixtures of colloidal particles, we assume we have K species of particles, each being characterized by the particle size l_α, $\alpha = 1, \ldots, K$. Finite size of the cell and steric repulsion between particles are taken into account by the exclusion constraint for each cell with capacity k, which is

$$\sum_{\alpha=1}^{K} n_\alpha l_\alpha \leqslant k, \tag{1}$$

where n_α is the number of particles of species α contained in the cell.

The simplest way how the pore as in Fig. 1(a) can be discretized into cells is the asymmetric comblike structure sketched in Fig. 1(b). There are two types of cells. The cells of the first type [one of them is denoted by the letter "s" in Fig. 1(b)] form a linear chain which will be called backbone. The cells of the second type (one of them is denoted by the letter "z" in Fig. 1(b); the meaning of the letters s and z will be clear later) complement the backbone by a sequence of dead ends of unit length. Each cell in the backbone is connected to exactly one cell of the second type. We shall call the cells of the second type pockets. The pockets are not connected directly one to another, but can communicate indirectly through the backbone.

Particles can jump from one cell to the other, provided the cells are directly connected. This means that particles can jump from a cell on the backbone to the two nearest-neighbor cells on the backbone. This is indicated in Fig. 1(b) by the corresponding right- and left-hand jump rates a and b. A particle in the backbone cell can also jump to the single pocket cell attached to it (indicated by rate c) and conversely, a particle can jump from the attached pocket to the backbone (as indicated by rate d). For further convenience, we shall fix the nomenclature so that the pair of cells consisting of one cell at the backbone and the pocket cell attached to it will be called a site. Therefore, the system consists of a linear chain of sites.

The second ingredient (after the geometry) of our model is the dynamics of the particles. In reality, the movement of the colloid particles has a deterministic and a stochastic component. The deterministic part comes from the hydrodynamic driving, which is known uniquely as long as the flow of the fluid is determined (provided the flow is laminar). The stochastic part is the Brownian motion, which depends on particle size, temperature, and fluid viscosity. Instead, in our model the movement of particles is purely stochastic, and the deterministic component of the real movement is taken into account in the model by a bias in jump rates between cells.

Therefore, the dynamics of the model is parametrized by a set of jump rates. For each of the K species of particles, we have four rates, namely, left and right jump rates along the backbone and jump rates to and from the pocket. The only constraint the particles must keep is the inequality (1) which must be satisfied at all cells. Jumps which would violate this constraint are forbidden. This is the generalization of the exclusion principle of the ASEP model, in which at most one particle at each site is allowed.

We shall denote the length of the backbone L (so that there are $2L$ cells in total) and always assume periodic boundary conditions.

As our main concern is with separation of particles by size, and at the same time we want to keep the model simple enough, the core results will contain particles of two species, i.e., $K = 2$. Their sizes will be simply $l_1 = 1$ (small particles) and $l_2 = 2$ (big particles). With a few exceptions (specified explicitly later), we shall keep the convention that upper-case symbols (rates, currents, etc.) pertain to big particles, while lower-case symbols are used for small particles.

B. Exactly solvable case

If our model contains only small particles and, moreover, if the capacity of the cells in the backbone is unity, $k = 1$, but the capacity q of the pockets can be arbitrary, we can exactly calculate the stationary many-particle state. The configurations are specified by the collection of occupations numbers $(s|z) = \{(s_i|z_i)\}$ where $s_i = 0, 1$ and $z_i = 0, 1, \ldots, q$ are the particle numbers in the ith backbone cell and in the attached pocket, respectively.

Stochastic transitions have the form of random jumps of particles both between neighboring backbone cells and between a backbone cell and the attached pocket, always respecting their capacities. In particular, the transition rate $W((s'|z') \leftarrow (s|z)) = a$ whenever a particle jumps from an ith backbone cell to the $(i+1)$th backbone cell, i.e., for $s_i = 1 - s_{i+1} = 1$, $s'_i = 1 - s'_{i+1} = 0$, and $s'_j = s_j$ for all other backbone cells, with the pocket configuration remaining untouched ($z' = z$). Analogously, the transition rate for the opposite jump, i.e., from the $(i+1)$th backbone cell to the ith one is denoted by b. A particle can also jump from the ith backbone cell to the attached pocket with rate c and the opposite process occurs with rate $d\, z_i$; note that it is proportional to the number of particles in the pocket.

We will show that the stationary distribution does not depend on the jump rates a and b, therefore it coincides with the stationary distribution of the detailed balanced dynamics ($a = b$). The latter is to be the equilibrium distribution of a system with L ground states (the backbone cells) and L excited states (the pockets), which in the grand-canonical setting takes the factorized form

$$P(s|z) = \prod_{i=1}^{L} [p(s_i)\, \bar{p}(z_i)], \tag{2}$$

where the marginal distributions in the backbone cells and the pockets, respectively, are

$$p(s_i) = \frac{\lambda^{s_i}}{1+\lambda}, \quad \bar{p}(z_i) = \frac{1}{\Xi(\lambda)} \frac{(\lambda\gamma)^{z_i}}{z_i!} \tag{3}$$

with $\gamma = c/d$ and $\Xi(\lambda) = \sum_{n=0}^{q} (\lambda\gamma)^n/n!$. In this ansatz we have used that the logarithmic ratio $\ln(d/c) = -\ln\gamma$ can be interpreted as the effective energy difference (with unit temperature) between the ground (backbone) and the excited (pocket) states. The averaged density of particles is then

$\rho_1 = \langle s_i \rangle + \langle z_i \rangle$ or

$$\rho_1 = \frac{\lambda}{1+\lambda} + \lambda \frac{d \ln \Xi(\lambda)}{d\lambda}. \tag{4}$$

We remark that by conditioning the distribution (2) on a fixed total number of particles $\sum_i (s_i + z_i) = \rho_1 L$, which is invariant under the dynamics, we would obtain the canonical form of distribution (no longer dependent on λ that cancels out). However, for convenience we stick to the factorized grand-canonical form (2) in the sequel, and we prove that it indeed provides the stationary distribution of the driven dynamics (i.e., for $a \neq b$, in general).

The stationary condition

$$\sum_{(s',z')} \mathcal{J}((s'|z') \leftarrow (s|z)) = 0 \tag{5}$$

expressed in words requires that the sum of all probability currents from any configuration $(s|z)$ is zero. There are four types of particle jumps: to or from the pocket (denoted by indices $\uparrow$ and $\downarrow$) and to the right or to the left along the backbone (denoted by indices $\rightarrow$ and $\leftarrow$). Therefore the stationarity condition can be written in the simplified form

$$\sum_i [\mathcal{J}_i^{\uparrow} + \mathcal{J}_i^{\downarrow} + \mathcal{J}_i^{\rightarrow} + \mathcal{J}_i^{\leftarrow}](s|z) = 0. \tag{6}$$

The first term $\mathcal{J}_i^{\uparrow}(s|z)$ can be nonzero only if the configuration $(s|z)$ satisfies $s_i = 1$, $z_i < q$, and it counts the probability current between this configuration and the configuration $(s'|z')$ such as $s'_i = 0$, $z'_i = z_i + 1$ (all other occupations unchanged), which equals

$$\mathcal{J}_i^{\uparrow}(s|z) = c\, P(s|z) - d(z_i + 1) P(s'|z'). \tag{7}$$

However, this is always zero since from (2) and (3) we have

$$\frac{P(s|z)}{P(s'|z')} = \frac{z_i + 1}{\gamma}. \tag{8}$$

By the same reasoning, $\mathcal{J}_i^{\downarrow}(s|z) = 0$ for the probability current between any $(s|z)$ such that $s_i = 0$ and $z_i > 0$ and $(s'|z')$ defined by $s'_i = 1$, $z'_i = z_i - 1$ (and the rest unchanged). Together it verifies the detailed balance condition for all transitions to and from the pockets, which is also intuitively clear from the geometry.

On the other hand, for the jumps to the right along the backbone we need $s_i = 1 - s_{i+1} = 1$ and the new configuration is $s'_i = 1 - s'_{i+1} = 0$ (and the rest unchanged). Since $P(s'|z') = P(s|z)$, the probability current between these two configurations is

$$\mathcal{J}_i^{\rightarrow}(s|z) = (a - b) P(s|z) s_i (1 - s_{i+1}). \tag{9}$$

Analogously, $\mathcal{J}_i^{\leftarrow}(s|z) = (b - a) P(s|z)$ whenever $s_i = 1 - s_{i-1} = 0$ and zero otherwise. Their sum can be conveniently written in the form

$$(\mathcal{J}_i^{\rightarrow} + \mathcal{J}_{i+1}^{\leftarrow})(s|z) = (a - b)(s_i - s_{i+1}) P(s|z) \tag{10}$$

from which the stationarity (5)–(6) immediately follows by summing over all cells $i = 1, \ldots, L$ and by using the periodic boundary conditions.

The stationary particle current is given by

$$j = \sum_{(s|z)} [\mathcal{J}_i^{\rightarrow} - \mathcal{J}_{i+1}^{\leftarrow}](s|z) = (a - b)\langle s_i \rangle (1 - \langle s_{i+1} \rangle) \tag{11}$$

(independently of i). In terms of the fugacity $\lambda(\rho_1, \gamma)$, the current reads $j = (a - b)\lambda/(1 + \lambda)^2$. Since the driving reversal corresponds to the transformation $a \leftrightarrow b$ together with $c \leftrightarrow d$, we can also calculate the ratchet current (for a flashing ratchet slowly switching between the positive and negative driving regimes) as

$$j_{\mathrm{rat}} = \frac{1}{2}(j + j^*) = \frac{a - b}{2}\left[\frac{\lambda}{(1+\lambda)^2} - \frac{\lambda^*}{(1+\lambda^*)^2}\right], \tag{12}$$

where $\lambda^* = \lambda(\rho_1, 1/\gamma)$ is the fugacity in the driving-reversed case and j^* is the corresponding particle current. The ratchet current as a function of the density of small particles can be obtained by inversion of the relation (4).

C. Strategies for general case

1. Monte Carlo simulation

In a generic case, there is no exact solution available and there is no easy hope for any, because as soon as $k > 1$ at the backbone the system is very likely to be nonintegrable. A natural choice is a direct numerical Monte Carlo (MC) simulation, which we implement using a cellular-automata approach. At each moment of the discrete simulation time the state of the system is described by the occupation numbers of particles of each species in each cell. We denote the set of occupation numbers by $\{\binom{z_i Z_i}{s_i S_i}\}$, where the numbers at the bottom denote the occupation numbers at the ith backbone cell, while the numbers on the top denote the occupation numbers at the pocket attached to the ith backbone cell. We shall keep the convention that the letters "z" correspond to the pockets and letters "s" correspond to the backbone. At the same time, capital letters denote occupation by big particles, and lowercase letters denote occupation by small particles. The site index i runs from 1 to L.

Transition probabilities between states of the system $W[\{\binom{z_i Z_i}{s_i S_i}\} \leftarrow \{\binom{z'_i Z'_i}{s'_i S'_i}\}]$ are deduced from the probabilities of individual processes which always affect at most two neighboring sites. Therefore, for the nondiagonal elements of the transition matrix we have

$$\begin{aligned} W\left[\left\{\binom{z_i Z_i}{s_i S_i}\right\} \leftarrow \left\{\binom{z'_i Z'_i}{s'_i S'_i}\right\}\right] \\ = \frac{\Delta_m}{L} \sum_{m=1}^{L} W_2\left[\binom{z_m Z_m}{s_m S_m}\binom{z_{m+1} Z_{m+1}}{s_{m+1} S_{m+1}}\right. \\ \left. \leftarrow \binom{z'_m Z'_m}{s'_m S'_m}\binom{z'_{m+1} Z'_{m+1}}{s'_{m+1} S'_{m+1}}\right], \end{aligned} \tag{13}$$

where $\Delta_m = \prod_{i, i\neq m, i\neq m+1} \delta_{s_i, s'_i} \delta_{S_i, S'_i} \delta_{z_i, z'_i} \delta_{Z_i, Z'_i}$. In the following we shall also denote $\chi_k(s, S) = 1$ if $0 \leqslant s$ and $0 \leqslant S$ and $s + 2S \leqslant k$. Otherwise we put $\chi_k(s, S) = 0$.

The matrix W_2 describes the probabilities of elementary jumping processes. For example, for a jump of a small particle to the right on the backbone we have

$$\begin{aligned} W_2\left[\binom{z_1 Z_1}{s_1 S_1}\binom{z_2 Z_2}{s_2 S_2} \leftarrow \binom{z_1 Z_1}{s_1 + 1 S_1}\binom{z_2 Z_2}{s_2 - 1 S_2}\right] \\ = \frac{1}{\nu}(s_1 + 1) a\ \chi_k(s_2, S_2). \end{aligned} \tag{14}$$

The list of all nonzero off-diagonal elements in the matrix W_2 is given in Appendix A.

The diagonal element of the transition matrix W is computed so that the matrix is stochastic, i.e., the sum of probabilities over all final states gives 1. The precise value of the constant ν is inessential in the simulation, except for the requirement that all elements of W are probabilities, i.e., fall into the interval [0,1]. For example, we can use $\nu = k(a + A + b + B + c + C + d + D)$. On the basis of these transition probabilities, we run a standard Monte Carlo simulation.

2. Mean-field approximation

Besides direct numerical simulation, we shall use the mean-field (MF) approximation. Details of the MF calculations will be thoroughly explained later. Here we just sketch the general approach. In the approximation, we want to keep correlations between the cell at the backbone and the pocket cell attached to it. These two cells form a single site. We neglect the correlations between different sites, assuming that the full probability distribution of all configurations factorizes into product of probabilities of configurations of individual sites. As we also suppose that the system is uniform, i.e., all sites are equivalent, we obtain a set of equations for the probabilities of configurations of one site. For $k = 3$, which will be the typical case studied here, there are 36 configurations. However, their probabilities are not all independent. Taking into account three constraints (one for unit total probability and two imposed by fixed number of particles of each species), we end with the set of 33 quadratic equations, which are then solved numerically. In the following sections we shall investigate specific situations, starting with the simplified ones (with lower number of independent equations). Comparison with corresponding results of Monte Carlo simulations will be provided in parallel.

III. PRELIMINARY CALCULATIONS

Before going to the full model with pockets, let us look first at several simpler situations. We shall omit the pockets, so that the particles can hop only along a linear chain, but suppose the cell capacity k is larger than 1. This feature generalizes the ASEP model.

A. One species of particles

1. Jump rates

In our analytic calculations, we shall work in continuous-time description. When we compare stationary-state properties with discrete-time Monte Carlo simulations, such distinction in the treatment of time plays no role, as long as probabilities and rates are properly matched one to the other.

Let us first simplify the model further by assuming just one species of particles, namely the small ones. The particle can jump to the right or to the left. The only condition is that the occupation s of any site must be $s \leqslant k$. We can introduce general jump rates depending on the occupation of the site. From a site occupied by s particles, one particle can jump to the right with probability a_s and to the left with probability b_s. If the particles do not interact, besides the steric constraint

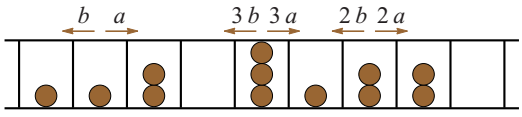

FIG. 2. Generalized ASEP model with the cell capacity $k = 3$; the rates are shown as given by Eq. (15). The probability that a particle jumps from a site occupied by s particles is proportional to s. This means that particles do not interact beyond the steric repulsion.

$s \leqslant k$, it is natural to let

$$a_s = sa, \quad b_s = sb. \tag{15}$$

This is the choice we shall use in most of the calculations and which also corresponds to our Monte Carlo simulations. However, as it will be clear later, our theory works equally well for any choice of the dependence of a_s and b_s on s. For example, we could investigate "sticky" particles, where a_s and b_s grow slower than linear with s. We illustrate the model for $k = 3$ in Fig. 2.

2. Chain of master equations

For small particles only and cell capacity k, each site can be in one of the $k + 1$ states denoted by the site occupation s. The configuration of the whole chain is the set of occupation numbers. The probability of the configuration $\{s_i\}$ will be denoted $P(\{s_i\})$. We suppose that these probabilities are invariant with respect to spatial translations. Then we can extract the one-site and two-site probabilities which do not depend on position:

$$P_s^{(1)} = \sum_{\{s_i\}} \frac{1}{L} \sum_{m=1}^{L} \delta_{s_m,s} P(\{s_i\}),$$

$$P_{ss'}^{(2)} = \sum_{\{s_i\}} \frac{1}{L} \sum_{m=1}^{L} \delta_{s_m,s} \delta_{s_{m+1},s'} P(\{s_i\}). \tag{16}$$

We can write an exact master equation for the one-site probabilities as follows. As a first step we construct an evolution equation for this one-site probability by explicitly analyzing possible jump processes. The change of $P_s^{(1)}$ in time is caused by jumps occurring on the left (L) and right (R) bonds connecting this site to its two neighbors,

$$\frac{d}{dt} P_s^{(1)} = x_{\mathrm{L}} + x_{\mathrm{R}}. \tag{17}$$

Each jump can be of the loss (−) or gain (+) type

$$x_{\mathrm{L}} = x_{\mathrm{L}}^{-} + x_{\mathrm{L}}^{+},$$
$$x_{\mathrm{R}} = x_{\mathrm{R}}^{-} + x_{\mathrm{R}}^{+}. \tag{18}$$

It is convenient to express these terms through functions l and u which select appropriate two-site states allowed for each s:

$$\begin{aligned} x_{\mathrm{L}}^{-} &= -b_s l_s^{\mathrm{L}} - \tilde{\delta}_{s,k} u_s^{\mathrm{L}}, \\ x_{\mathrm{L}}^{+} &= \tilde{\delta}_{s,k} b_{s+1} l_{s+1}^{\mathrm{L}} + \tilde{\delta}_{s,0} u_{s-1}^{\mathrm{L}}, \\ x_{\mathrm{R}}^{-} &= -a_s l_s^{\mathrm{R}} - \tilde{\delta}_{s,k} u_s^{\mathrm{R}}, \\ x_{\mathrm{R}}^{+} &= \tilde{\delta}_{s,k} a_{s+1} l_{s+1}^{\mathrm{R}} + \tilde{\delta}_{s,0} u_{s-1}^{\mathrm{R}}. \end{aligned} \tag{19}$$

Here factors $\tilde{\delta}_{s,s'} = 1 - \delta_{s,s'}$ are used to exclude the terms for states $s = \{0, k\}$ where necessary. Equalities $a_0 = b_0 = 0$

are also implied. The selective functions l and u are defined through two-site probabilities as follows:

$$l_s^{\mathrm{L}} = \sum_{s'=0}^{k-1} P_{s's}^{(2)}, \quad u_s^{\mathrm{L}} = \sum_{s'=1}^{k} a_{s'} P_{s's}^{(2)},$$
$$l_s^{\mathrm{R}} = \sum_{s'=0}^{k-1} P_{ss'}^{(2)}, \quad u_s^{\mathrm{R}} = \sum_{s'=1}^{k} b_{s'} P_{ss'}^{(2)}. \tag{20}$$

Functions $l_s^{\mathrm{L}}, l_s^{\mathrm{R}}$ refer to jumps from the site in state s, whereas u_s^{L}, u_s^{R} describe jumps onto this site. The context of defining these functions for one-site states is similar to the one for many-site states discussed in the formulation of the pairwise balance for the drop-push model [91]. It is easy to notice that the "R" functions change to the "L" ones, if indices of $P^{(2)}$ are permuted and simultaneous substitution $b_{s'} \to a_{s'}$ is made. The same holds for $x_{\mathrm{R}}^{\mp}$ and $x_{\mathrm{L}}^{\mp}$.

Expressions (17) through (20) together constitute the master equation for the one-site probabilities. By analogy, similar equation can be obtained for two-site, three-site, etc., probabilities, thus producing a chain of equations familiar from many branches of statistical physics. We need the probabilities beyond the one-site ones in order to calculate measurable quantities. For example, from the two-site probabilities we obtain the current along the bond between two neighboring sites as

$$j = \sum_{s=1}^{k} \sum_{s'=0}^{k-1} a_s P_{ss'}^{(2)} - \sum_{s=0}^{k-1} \sum_{s'=1}^{k} b_{s'} P_{ss'}^{(2)}. \tag{21}$$

3. Mean-field approximation

The simplest closure of the chain of master equations is obtained by assuming factorization of two-site probabilities

$$P_{ss'}^{(2)} \approx P_s^{(1)} P_{s'}^{(1)}. \tag{22}$$

This is the mean-field (MF) approximation, neglecting the correlations between neighboring sites. Moreover, note that not only correlations are absent in the MF approximation, but also the asymmetry $P_{ss'}^{(2)} \neq P_{s's}^{(2)}$, which may play important role in a driven system, disappears in MF approach.

This way we obtain closed set of equations for the $k+1$ probabilities $P_s^{(1)}$. Hence, from now on we drop the superscript "(1)," as there is no danger of confusion.

The periodic boundary conditions imply that the number of particles in the system is conserved. Therefore, the average density of particles ρ_1 is constant and the one-site probabilities satisfy two linear conditions $\sum_{s=0}^{k} P_s = 1$ and $\sum_{s=0}^{k} s P_s = \rho_1$. This reduces the number of independent equations to $k-1$.

Owing to approximation (22) the selective functions reduce to

$$l_s^{\mathrm{L}} = l_s^{\mathrm{R}} \approx P_s \sum_{s'=0}^{k-1} P_{s'},$$
$$u_s^{\mathrm{L}} \approx P_s \sum_{s'=1}^{k} a_{s'} P_{s'},$$
$$u_s^{\mathrm{R}} \approx P_s \sum_{s'=1}^{k} b_{s'} P_{s'}. \tag{23}$$

We are interested in a steady state, defined by $dP_s/dt = 0$. From (17) and (22): it follows that the stationary master equation has the form

$$0 = (a+b)[(-h_s P_s + \tilde{\delta}_{s,k} h_{s+1} P_{s+1}) l + (-\tilde{\delta}_{s,k} P_s + \tilde{\delta}_{s,0} P_{s-1}) u], \tag{24}$$

where $h_s = (a_s + b_s)/(a+b)$ are the reduced rates and

$$l = \sum_{s'=0}^{k-1} P_{s'}, \quad u = \sum_{s'=1}^{k} h_{s'} P_{s'}. \tag{25}$$

The current defined by Eq. (21) can be written as

$$j = \sum_{s=1}^{k} (a_s - b_s) P_s l. \tag{26}$$

It is simplified to $j = (a-b)ul$, if $a_s/a = b_s/b$.

The set of $k+1$ quadratic equations (24) for P_s written as

$$0 = h_1 P_1 l - P_0 u,$$
$$0 = (-h_1 P_1 + h_2 P_2) l + (-P_1 + P_0) u,$$
$$\ldots,$$
$$0 = -h_k P_k l + P_{k-1} u$$

is to be solved with respect to the probabilities. However, it is reducible to one equation. We simplify it by successive adding to obtain $h_{s+1} P_{s+1} l - P_s u = 0$ for each s, from which k quasilinear relations follow: $P_s = \phi h_{s+1} P_{s+1}$, where $\phi = l/u$. P_s for any $s < k$ can be expressed through P_k as

$$P_s|_{s<k} = \phi^{k-s} h_{s+1} h_{s+2} \cdots h_k P_k. \tag{27}$$

Using this formula in the normalization condition yields P_k in terms of ϕ:

$$P_k = \left[\sum_{s=0}^{k} h_{s+1} \cdots h_k \phi^{k-s} \right]^{-1}. \tag{28}$$

Note that in the most interesting case (15) we have simply $h_s = s$ and the probabilities are equal to truncated Poisson distribution

$$P_s = P_0 \frac{\phi^{-s}}{s!} \quad \text{for } s \leqslant k,$$
$$P_s = 0 \quad \text{for } s > k. \tag{29}$$

Equations (27) and (28) derived from the set of stationary equations (24) express all the probabilities through ϕ. However, the neglect of nearest-neighbor correlations by the use of Eq. (22) has resulted in that these expressions coincide with their equilibrium counterparts [80,83] written in terms of the fugacity, $\lambda = 1/\phi$, which can be obtained from the grand canonical ensemble for $a = b$. For the ASEP model ($k = 1$) the stationary solution (29) is exact; cf. Sec. II B (without pockets). More generally, for $k > 1$ and under the assumption $a_s/b_s = a/b$, the MF solution (27) coincides with the exact stationary distribution of the corresponding zero-range process [92].

The equation for ϕ is derived by multiplying the normalization condition by ρ_1 and subtracting from the density-fixing

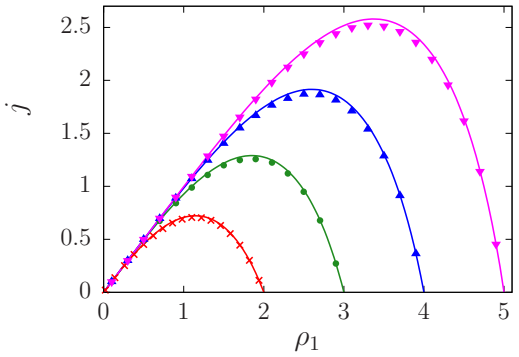

FIG. 3. Particle current for the generalized ASEP model with small particles only. Points represent Monte Carlo simulation data, lines correspond to mean-field approximation. The site capacity is $k = 2$ (×), $k = 3$ (•), $k = 4$ (▲), and $k = 5$ (▼). The hopping rates are $a = 1$, $b = 0$.

condition: $\sum_{s=0}^{k} P_s(\rho_1 - s) = 0$. Substitution of Eqs. (27) into this relation yields

$$\sum_{s=0}^{k} \frac{\rho_1 - s}{h_1 h_2 \cdots h_s} \phi^{k-s} = 0. \tag{30}$$

The rates satisfying Eq. (15) yield $h_s = s$, and Eq. (30) is reduced to

$$\sum_{s=0}^{k} \frac{\rho_1 - s}{s!} \phi^{k-s} = 0, \tag{31}$$

whereas the current is

$$j = (a - b)(1 - P_k)\rho_1. \tag{32}$$

We can see that the current depends on the rates a and b only through the multiplicative factor $(a - b)$ in (32). The occupation probabilities P_s do not depend on the rates at all. This is the consequence of (15). For other choices of the rates a_s, b_s this may not be true.

4. Comparison with Monte Carlo simulations

We can easily solve Eq. (31) and from the solution compute the current (32). The results were compared with direct Monte Carlo (MC) simulation using the transition probabilities (13) appropriately simplified for the case without pockets and in presence of small particles only. The results are shown in Fig. 3 for the cell capacity $k = 2, 3, 4$, and 5. We can see that for $k = 2$ the mean-field results are barely distinguishable from the MC simulation. When we increase k, the MF deviation from MC results increases, but the agreement still remains very good. This means that the correlation effects, neglected in MF approximation, remain very small. We shall see in the next section that the situation changes dramatically when big particles are also present.

B. Two species of particles

1. Jump rates

Now we add big particles. The size of these particles is $l_2 = 2$, and the number of big particles on a site will be

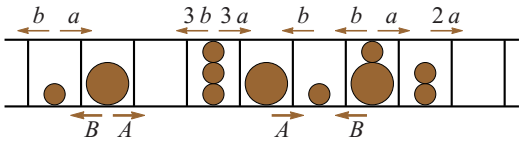

FIG. 4. Generalized ASEP model with two species of particles and cell capacity $k = 3$.

denoted by capital letters. If there are s small particles and S big particles on the same site, the constraint $s + 2S \leqslant k$ must be satisfied. In analogy with jump rates of small particles, we denote by A_S and B_S the rates at which one big particle jumps from a site occupied by S big particles to the right and to the left, respectively. Also in analogy to (15), when comparing the MF results with MC simulations we shall use

$$A_S = SA, \quad B_S = SB, \tag{33}$$

which holds for particles which interact only by steric repulsion. However, our calculations will hold for any form of the dependence of the rates on S. The model is depicted schematically in Fig. 4.

2. Mean-field approximation

The one- and two-site probabilities for occupation by s small particles and S big particles will be denoted $P^{(1)}_{sS}$ and $P^{(2)}_{sS;s'S'}$, respectively. The master equation for these probabilities can be constructed in the same way as it was done in the preceding section for the one-species case. (See Appendix B 1 for details.) We shall directly proceed to the mean-field approximation

$$P^{(2)}_{sS;s'S'} \approx P^{(1)}_{sS} P^{(1)}_{s'S'}. \tag{34}$$

We also drop the superscript "(1)" in the following, as we did in the one-species case.

In the stationary state $dP_{sS}/dt = 0$ and we obtain a set of quadratic equations for the one-site probabilities. In the special case $k = 3$ which will be analyzed in detail, we have six quadratic equations. The probabilities must also satisfy the conditions implied by fixed density ρ_1 of small particles and density ρ_2 of big particles

$$\sum_{s,S}^{(k)} P_{sS} = 1, \quad \sum_{s,S}^{(k)} s\, P_{sS} = \rho_1, \quad \sum_{s,S}^{(k)} S\, P_{sS} = \rho_2, \tag{35}$$

where (k) in upper limits of the sums denotes restriction $s + 2S \leqslant k$. In fact, the densities of small and big particles, ρ_1 and ρ_2, have to satisfy similar inequality $\rho_1 + 2\rho_2 \leqslant k$.

The MF steady-state master equation for P_{sS} is as follows:

$$\begin{aligned} 0 = (a + b)\{&[-h_s P_{sS} + \tilde{\delta}_{s+2S,k} h_{s+1} P_{s+1,S}] l \\ &+ [-\tilde{\delta}_{s+2S,k} P_{sS} + \tilde{\delta}_{s,0} P_{s-1,S}] u \\ &+ [-H_S P_{sS} + \tilde{\tilde{\delta}}_{s+2S,k} H_{S+1} P_{s,S+1}] L \\ &+ [-\tilde{\tilde{\delta}}_{s+2S,k} P_{sS} + \tilde{\delta}_{S,0} P_{s,S-1}] U\}, \end{aligned} \tag{36}$$

where $H_S = (A_S + B_S)/(a + b)$ and the factor $\tilde{\tilde{\delta}}_{s+2S,k} = 1 - \delta_{s+2S,k} - \delta_{s+2S,k-1}$ ensures correct treatment of highly occupied states for big particles. The MF selective functions l, L

are defined in the Appendix, Eqs. (B8) and (B10), whereas the MF expressions for u and U read

$$u = \sum_{s',S'}^{(k)} h_{s'} P_{s'S'}, \quad U = \sum_{s',S'}^{(k)} H_{S'} P_{s'S'}. \tag{37}$$

The MF currents of small and big particles are

$$j = \sum_{s,S}^{(k)} (a_s - b_s) P_{sS}\, l, \quad J = \sum_{s,S}^{(k)} (A_S - B_S) P_{sS}\, L. \tag{38}$$

For details, see the Appendix, Eqs. (B5) and (B6).

Let us consider the case $k = 3$ for which an additional restriction $\rho_2 \leqslant 1$ takes place. Stationary MF master equations for P_{sS} follow from Eq. (36):

$$\begin{aligned}
P_{00} &: 0 = h_1 P_{10} l - P_{00} u + H_1 P_{01} L - P_{00} U, \\
P_{10} &: 0 = (-h_1 P_{10} + h_2 P_{20}) l + (-P_{10} + P_{00}) u \\
&\quad + H_1 P_{11} L - P_{10} U, \\
P_{20} &: 0 = (-h_2 P_{20} + h_3 P_{30}) l + (-P_{20} + P_{10}) u, \\
P_{30} &: 0 = -h_3 P_{30} l + P_{20} u, \\
P_{01} &: 0 = h_1 P_{11} l - P_{01} u - H_1 P_{01} L + P_{00} U, \\
P_{11} &: 0 = -h_1 P_{11} l + P_{01} u - H_1 P_{11} L + P_{10} U,
\end{aligned} \tag{39}$$

where

$$\begin{aligned}
l &= P_{00} + P_{10} + P_{20} + P_{01}, \\
u &= h_1 P_{10} + h_2 P_{20} + h_3 P_{30} + h_1 P_{11}, \\
L &= P_{00} + P_{10}, \\
U &= H_1 P_{01} + H_1 P_{11}.
\end{aligned} \tag{40}$$

Again, the problem can be reduced to one equation for the quantity $\phi = l/u$ (see Appendix B 2). The equation is

$$\begin{aligned}
&\rho_1 \phi^4 + \frac{2\rho_1 - 1}{h_1} \phi^3 + \frac{(h_1 + h_2)\rho_1 + 2h_1\rho_2 - 2h_1 - h_2}{h_1^2 h_2} \phi^2 \\
&+ \frac{(h_1 + h_3)\rho_1 + (3h_1 + h_3)\rho_2 - 3h_1 - 2h_2}{h_1^2 h_2 h_3} \phi \\
&+ \frac{\rho_1 + 2\rho_2 - 3}{h_1^2 h_2 h_3} = 0.
\end{aligned} \tag{41}$$

Note that the equation does not depend on the jump rates of big particles. The probabilities and the currents are calculated from the solution to Eq. (41) as explained in Appendix B 2. For the rates taken as in Eq. (15) the final equation is reduced to

$$\begin{aligned}
&\rho_1 \phi^4 + (2\rho_1 - 1)\phi^3 + \frac{3\rho_1 + 2\rho_2 - 4}{2} \phi^2 \\
&+ \frac{4\rho_1 + 6\rho_2 - 9}{6} \phi + \frac{\rho_1 + 2\rho_2 - 3}{6} = 0.
\end{aligned} \tag{42}$$

From the solution of this equation we extract the currents of small and big particles according to (38), which is then compared with MC simulations.

3. *Comparison with Monte Carlo simulations*

The allowed range of densities of small and big particles is limited by inequalities $0 \leqslant \rho_2 \leqslant 1$, $0 \leqslant \rho_1 \leqslant 3$, and $\rho_1 + 2\rho_2 \leqslant 3$. It is depicted schematically in Fig. 5, where we can distinguish several special regimes. Line I with $\rho_1 \in [0; 3]$, $\rho_2 = 0$ represents the one-species generalized ASEP with $k = 3$ which has been considered above and the results are shown in Fig. 3. Line II with $\rho_1 = 0$, $\rho_2 \in [0; 1]$, corresponds to the classical ASEP model of big particles. Correlations are known to be absent in the stationary state of this model on the ring while the current reads $J = (A - B)\rho_2(1 - \rho_2)$. There is also no correlation on line III with $\rho_1 \in [0; 1]$, $\rho_2 = 1$, where the big particles are immovable ($J = 0$) and the small particles behave like the ASEP with $j = (a - b)\rho_1(1 - \rho_1)$. The close-packing line represents mixtures of varying composition with currents j and J being equal to zero.

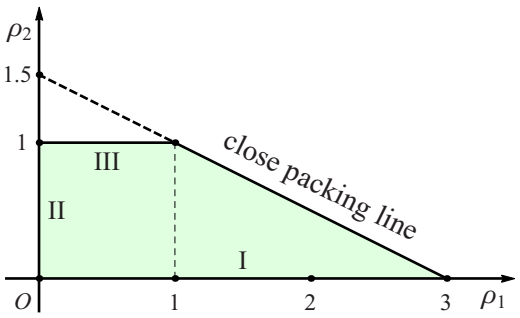

FIG. 5. The region of densities for the two-species generalized ASEP with $k = 3$.

Therefore, we expect that the correlations will diminish when we approach the edges of the allowed density region indicated in Fig. 5 and the MC simulation data will be close to MF results. On the contrary, in the interior part of the allowed density region we expect larger correlations and higher difference between MC and MF values.

We show in Fig. 6 dependence of the currents of big and small particles on the density of small as well as big particles. First, we can observe that the MF results always agree qualitatively with MC simulations. The trends, positions of the maxima, and exact intervals of density, within which the currents are nonzero, are all well reproduced. Quantitatively, though, there are often considerable differences, which call for explanation. Generally, the difference between the MF and MC results are due to correlations and the size of the deviations may serve as an estimate of the importance of these correlations. We can clearly see that the correlations are stronger for intermediate densities and tend to zero when the densities come close to lower or upper limits. This is most evident in Figs. 6(a) and 6(d), where we can see the dependence of the current of small particles on the density of small, and the current of big on the density of big particles, respectively. Let us look at Figs. 6(a) more carefully. Next to lower and upper limits of ρ_1, the agreement is very good. We can also see that when the density of big particles is large [$\rho_2 = 0.8$ in Fig. 6(a)] the agreement is quite good for any ρ_1, while for smaller ρ_2, the deviation is as large as 25% in the middle of the allowed ρ_1. This seems to be in contrast with the results presented in Fig. 3, where the dependence of j on ρ_1 for $\rho_2 = 0$ shows very good agreement of MF and MC results. The situation becomes more clear when looking at Fig. 6(b), where we can see the dependence of j

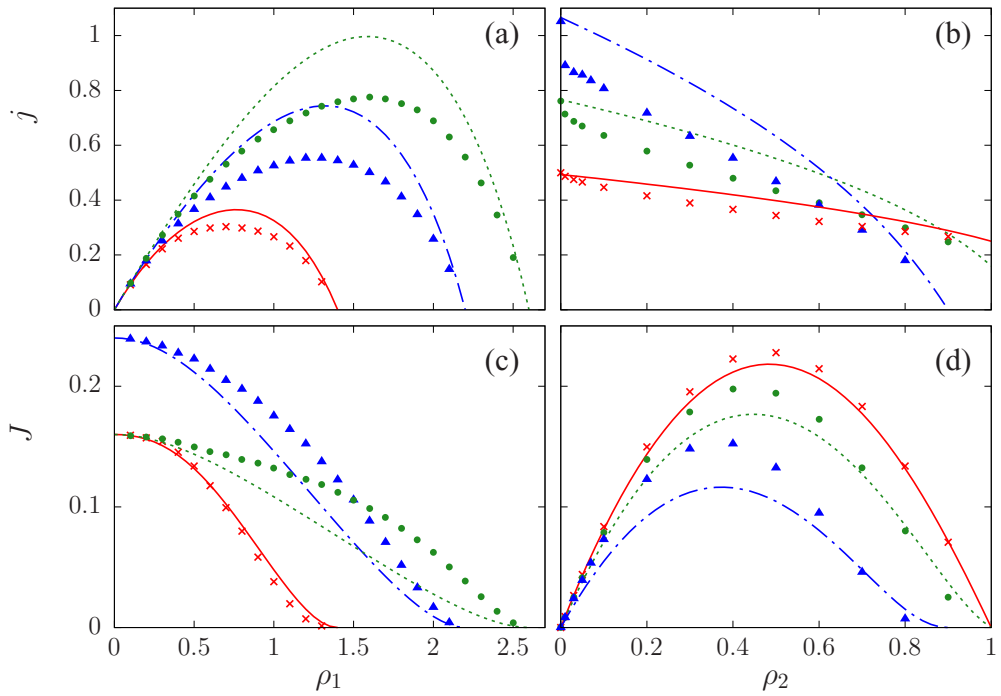

FIG. 6. Dependence of the current of small particles [panels (a) and (b)] and the current of big particles [panels (c) and (d)] on the density of small particles [panels (a) and (c)] and big particles [panels (b) and (d)], in the generalized ASEP model. The points represent numerical simulation data, the lines are results of mean-field approximation. The rates are $a = A = 1, b = B = 0$. The parameters in panels (a) and (c) are $\rho_2 = 0.8$ (×, solid line), $\rho_2 = 0.4$ (▲, dot-dashed line), $\rho_2 = 0.2$ (•, dotted line). The parameters in panels (b) and (d) are $\rho_1 = 0.5$ (×, solid line), $\rho_1 = 0.8$ (•, dotted line), $\rho_1 = 1.2$ (▲, dot-dashed line).

on ρ_2. We observe that at high values of ρ_2 the difference between MF and MC gradually diminishes. On the contrary, when ρ_2 approaches zero, the difference stays large, or even seems to increase. This needs a detailed view at what happens at very small concentration of big particles. Such detail is shown in Fig. 7. We can see that down to values as small as $\rho_2 = 0.005$ the current j seems to converge to a value significantly lower than the value observed at $\rho_2 = 0$ exactly. Only within very narrow region of very small concentrations of big particles we observe steep approach to the $\rho_2 = 0$ value. This implies that addition of a few big particles into the system of small particles induces significant correlations. In fact, it is not difficult to understand these correlations qualitatively. Even a single big particle acts as a "bottleneck" for small particles, slowing their movement locally. To see this effect, we calculated by MC simulations the pair correlation function

$$C(i-j) = \langle s_i S_j \rangle - \langle s_i \rangle \langle S_j \rangle, \tag{43}$$

where s_i and S_i denote the number of small and big particles present at the site i, respectively. In Fig. 8 we show the results

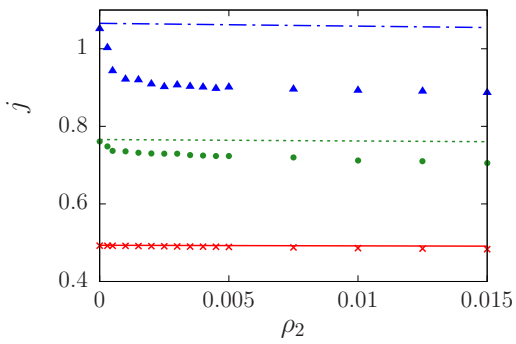

FIG. 7. Detail of the dependence of the current of small particles on the density of big particles, as shown in Fig. 6(b). The parameters are $\rho_1 = 0.5$ (×, solid line), $\rho_1 = 0.8$ (•, dotted line), $\rho_1 = 1.2$ (▲, dot-dashed line).

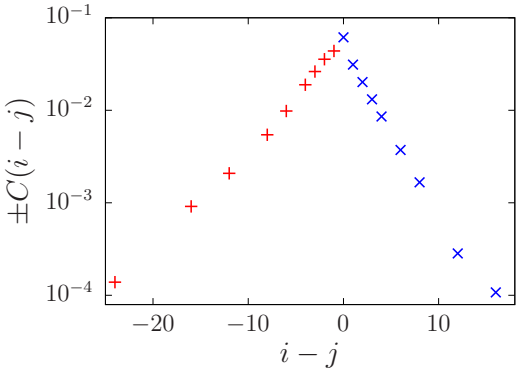

FIG. 8. Pair correlation function of the densities of big and small particles. The symbols distinguish the sign to be applied in front of the quantity C: + corresponds to the plus sign (i.e., correlation function is positive), and × corresponds to the minus sign (i.e., correlation function is negative). The average densities are $\rho_1 = 1.2$, $\rho_2 = 0.1$, the hopping rates are $a = 1, A = 0.5, b = B = 0$.

for a typical set of parameters. We can clearly see that behind a big particle, an exponentially decaying cloud of enhanced density of small particles is formed. At the same time, in front of the big particle, the density of small particles is depleted, also with an exponential decay.

This observation also provides a hint why the MF results for current of big particles are sometimes higher than MC results, while in other cases the opposite is true. Indeed, if small particles are depleted in front of the big one, as Fig. 8 indicates, the big particle jumps to the right with higher probability in comparison to uniform configurations with average density ρ_1 implied by MF approximation. This is in agreement with the observation that the MF current of big particles mainly underestimates the MC data, $J_{\mathrm{MF}} < J_{\mathrm{MC}}$ [Figs. 6(c) and 6(d)]. Overestimation takes place only when the both densities are high, $\rho_2 \geqslant 0.8$, $\rho_1 \geqslant 0.8$. On the contrary, big particles can only decrease the MC current of small ones and overall overestimation $j_{\mathrm{MF}} > j_{\mathrm{MC}}$ is similar to that of the model without big particles considered in the previous subsection.

IV. FULL MODEL WITH POCKETS

Let us now investigate the model introduced in Sec. II in full detail. The geometry is quasi-one-dimensional. The entity we shall call "site" consists of two cells, the first at the backbone and the second attached to the first as a pocket. Configuration of the site is specified by occupation numbers of both species of particles at both the backbone cell (s and S) and the pocket cell (z and Z). As always, capital letters belong to big particles, lowercase letters to small particles. In general, capacity k of the backbone cell may be different from the capacity q of the pocket cell. The restriction for the occupation numbers at each site is then $s + 2S \leqslant k$ and $z + 2Z \leqslant q$.

As in the case of jump rates along the backbone, also the jump rates to and from the pockets depend on the occupation of the cell from which the jump occurs. We shall denote them c_s, C_S for jumps to the pocket and d_z, D_Z for the jumps from the pocket. As before, for particles interacting only by steric repulsion we have

$$\begin{aligned} a_s &= sa, \quad A_S = SA, \\ b_s &= sb, \quad B_S = SB, \\ c_s &= sc, \quad C_S = SC, \\ d_z &= zd, \quad D_Z = ZD. \end{aligned} \tag{44}$$

A. One species of particles

Let us start with small particles only. The configuration of the site is $\binom{z}{s}$ where z is occupation of the pocket and s occupation of the backbone cell. As before, we can define one-site configuration probabilities $P^{(1)}_{sz}$, and assuming factorization of the two-site probabilities, we arrive at a closed set of equations in the mean-field approximation. These equations are complemented by the conditions of normalization and fixing the density

$$\sum_{s=0}^{k}\sum_{z=0}^{q} P^{(1)}_{sz} = 1, \quad \sum_{s=0}^{k}\sum_{z=0}^{q} (s+z) P^{(1)}_{sz} = \rho_1. \tag{45}$$

Probability $P^{(1)}_{sz}$ is governed by the following generalization of Eq. (17):

$$\frac{d}{dt} P^{(1)}_{sz} = x_{\mathrm{L}} + x_{\mathrm{R}} + y, \tag{46}$$

where x_{L} and x_{R} refer to jumps between sites, while y describes one-site pocket processes (see Appendix C 1 for details).

In a steady state, equality $dP^{(1)}_{sz}/dt = 0$ holds. Then Eq. (46) within the MF approximation and under periodic boundary conditions is reduced to

$$\begin{aligned} 0 = (a+b)\{&[-h_s P_{sz} + \tilde{\delta}_{s,k} h_{s+1} P_{s+1,z}] l \\ &+ [-\tilde{\delta}_{s,k} P_{sz} + \tilde{\delta}_{s,0} P_{s-1,z}] u\} \\ &- \tilde{\delta}_{z,q} c_s P_{sz} + \tilde{\delta}_{z,q} \tilde{\delta}_{s,0} d_{z+1} P_{s-1,z+1} \\ &+ \tilde{\delta}_{s,k} \tilde{\delta}_{z,0} c_{s+1} P_{s+1,z-1} - \tilde{\delta}_{s,k} d_z P_{sz}, \end{aligned} \tag{47}$$

where the superscript "(1)" has been omitted as before and we introduce

$$l = \sum_{s'=0}^{k-1}\sum_{z'=0}^{q} P_{s'z'}, \quad u = \sum_{s'=1}^{k} h_{s'} \sum_{z'=0}^{q} P_{s'z'}. \tag{48}$$

The current

$$j = \sum_{s=1}^{k} (a_s - b_s) l \sum_{z=0}^{q} P_{sz} \tag{49}$$

simplifies to

$$j = (a-b) u l \tag{50}$$

if the rates are given by (15).

The set of stationary master equations (47) can be reduced to one equation for $k = 1$; see Appendix C 2. Similar reduction to a single algebraic equation was shown in the cases without pockets, investigated in the previous sections. Here, though, for $k \geqslant 2$ such simple reduction is not possible in general case but still remains possible if the jump rates satisfy (44). (See Appendix C 3 for details.) In this special case and for $k = q = 3$ the final equation for $\phi = l/u$ reads [see also Eq. (C26)]

$$\begin{aligned} &\rho\phi^6 + (1+\gamma)(\rho-1)\phi^5 + \frac{1}{2}(1+\gamma)^2(\rho-2)\phi^4 \\ &+ \frac{1}{6}(1+\gamma)^3(\rho-3)\phi^3 + \frac{\gamma}{6}\left(1 + \frac{3}{2}\gamma + \gamma^2\right)(\rho-4)\phi^2 \\ &+ \frac{\gamma^2}{12}(1+\gamma)(\rho-5)\phi + \frac{\gamma^3}{36}(\rho-6) = 0 \end{aligned} \tag{51}$$

with $\gamma = c/d$. From the solution of this equation we reconstruct all the one-site probabilities and then compute the current.

B. Two species of particles

Now we turn to the case of two species. The capacities of backbone and pocket cells imply restrictions on the densities of small (ρ_1) and big (ρ_2) particles, namely, $\rho_1 + 2\rho_2 \leqslant k + q$. The one-site probabilities $P^{(1)}_{sS,zZ}$ satisfy three conditions

originating from fixed densities

$$\sum_{s,S}^{(k)}\sum_{z,Z}^{(q)} P^{(1)}_{sS,zZ} = 1,$$
$$\sum_{s,S}^{(k)}\sum_{z,Z}^{(q)} (s+z)\, P^{(1)}_{sS,zZ} = \rho_1,$$
$$\sum_{s,S}^{(k)}\sum_{z,Z}^{(q)} (S+Z)\, P^{(1)}_{sS,zZ} = \rho_2. \tag{52}$$

The master equation for the one-site probability is written in the form

$$\frac{d}{dt}P^{(1)}_{sS,zZ} = x + y + X + Y, \tag{53}$$

where x and X are related to jumps of small and big particles along the backbone and y and Y describe jumps of small and big particles to and from the pockets. Explicit expressions for them are given in Appendix D 1.

The mean-field approximation is performed as usual by factorizing two-site probabilities. At the same time we again drop the superscript "(1)." Then, in the MF approximation we have

$$x = (a+b)[(-h_s P_{sS,zZ} + \tilde{\delta}_{s+2S,k} h_{s+1} P_{s+1,S,zZ})l + (-\tilde{\delta}_{s+2S,k} P_{sS,zZ} + \tilde{\delta}_{s,0} P_{s-1,S,zZ})u],$$

$$X = (a+b)[(-H_S P_{sS,zZ} + \tilde{\tilde{\delta}}_{s+2S,k} H_{S+1} P_{s,S+1,zZ})L + (-\tilde{\tilde{\delta}}_{s+2S,k} P_{sS,zZ} + \tilde{\delta}_{S,0} P_{s,S-1,zZ})u]. \tag{54}$$

Functions l, L are given in Eqs. (D11) and (D13) while u, U are defined as follows:

$$u = \sum_{s',S'}^{(k)} h_{s'} \sum_{z',Z'}^{(q)} P_{s'S',z'Z'},$$
$$U = \sum_{s',S'}^{(k)} H_{S'} \sum_{z',Z'}^{(q)} P_{s'S',z'Z'}. \tag{55}$$

The MF currents of small and big particles read

$$j = \sum_{s,S}^{(k)} (a_s - b_s) l \sum_{z,Z}^{(q)} P_{sS,zZ},$$
$$J = \sum_{s,S}^{(k)} (A_S - B_S) L \sum_{z,Z}^{(q)} P_{sS,zZ}. \tag{56}$$

If $a_s/a = b_s/b$ and $A_S/a = B_S/b$ for all s and S, these are reduced to

$$j = (a-b)ul, \quad J = (a-b)UL. \tag{57}$$

The equations for stationary state can be simplified for rates satisfying (44). Using the same procedure as in one-species case (detailed in Appendix C 3), we arrive at a set of just two algebraic equations for the quantities $\phi = l/u$ and $\psi = U/L$ which are

$$\begin{aligned}
&\rho_1\phi^6 + (1+\gamma)[\rho_1-1]\phi^5 + \tfrac{1}{2}(1+\gamma)^2[\rho_1-2]\phi^4 + \tfrac{1}{6}(1+\gamma)^3[\rho_1-3]\phi^3 \\
&\quad + \tfrac{1}{6}\gamma\big(1+\tfrac{3}{2}\gamma+\gamma^2\big)[\rho_1-4]\phi^2 + \tfrac{1}{12}\gamma^2(1+\gamma)[\rho_1-5]\phi + \tfrac{1}{36}\gamma^3[\rho_1-6] \\
&\quad + \psi\big\{\rho_1\phi^6 + (1+\gamma)[\rho_1-1]\phi^5 + \gamma\big(1+\tfrac{1}{2}\gamma\big)[\rho_1-2]\phi^4 + \tfrac{1}{2}\gamma^2\big(1+\tfrac{1}{3}\gamma\big)[\rho_1-3]\phi^3 + \tfrac{1}{6}\gamma^3[\rho_1-4]\phi^2\big\} \\
&\quad + \Gamma\psi\big\{\rho_1\phi^6 + (1+\gamma)[\rho_1-1]\phi^5 + \tfrac{1}{2}(1+2\gamma)[\rho_1-2]\phi^4 + \tfrac{1}{6}(1+3\gamma)[\rho_1-3]\phi^3 + \tfrac{1}{6}\gamma[\rho_1-4]\phi^2\big\} \\
&\quad + \Gamma\psi^2\big\{\rho_1\phi^6 + (1+\gamma)[\rho_1-1]\phi^5 + \gamma[\rho_1-2]\phi^4\big\} = 0,
\end{aligned} \tag{58}$$

$$\begin{aligned}
&\rho_2\big\{\phi^6 + (1+\gamma)\phi^5 + \tfrac{1}{2}(1+\gamma)^2\phi^4 + \tfrac{1}{6}(1+\gamma)^3\phi^3 + \tfrac{1}{6}\gamma\big(1+\tfrac{3}{2}\gamma+\gamma^2\big)\phi^2 + \tfrac{1}{12}\gamma^2(1+\gamma)\phi + \tfrac{1}{36}\gamma^3\big\} \\
&\quad + (\rho_2-1)\psi\big\{\phi^6 + (1+\gamma)\phi^5 + \gamma\big(1+\tfrac{1}{2}\gamma\big)\phi^4 + \tfrac{1}{2}\gamma^2\big(1+\tfrac{1}{3}\gamma\big)\phi^3 + \tfrac{1}{6}\gamma^3\phi^2\big\} \\
&\quad + (\rho_2-1)\Gamma\psi\big\{\phi^6 + (1+\gamma)\phi^5 + \tfrac{1}{2}(1+2\gamma)\phi^4 + \tfrac{1}{6}(1+3\gamma)\phi^3 + \tfrac{1}{6}\gamma\phi^2\big\} \\
&\quad + (\rho_2-2)\Gamma\psi^2\big\{\phi^6 + (1+\gamma)\phi^5 + \gamma\phi^4\big\} = 0,
\end{aligned} \tag{59}$$

where $\gamma = c/d$ and $\Gamma = C/D$. From the solution of these equations, the one-site probabilities can be reconstructed straightforwardly (see Appendix D 1 for details).

C. Comparison with Monte Carlo simulations

We investigate the simplest nontrivial situation $k = 3$ and $q = 3$. The backbone and pocket cell capacities imply a restriction on the densities of small and big particles, namely, $\rho_1 + 2\rho_2 \leqslant 6$. Moreover, in this geometry there can be at most one big particle both in the backbone cell and in the pocket, therefore $\rho_2 \leqslant 2$. This defines the area of allowed densities.

We show in Figs. 9 and 10 the currents of small and big particles as functions of the density of small particles in comparison with direct MC simulations. We use the same value $\gamma = \Gamma$ for big and small particles. Again, we can see that in the limits $\rho_1 \to 0$ and ρ_1 approaching the maximum allowed value, the agreement between the MF and MC results is very good, while in the intermediate region the correlations cause marked deviations. This is the same behavior as in the case without pockets. In the dependence of the current of big particles we observe a remarkable feature. In the regime $\rho_2 < 1$, shown in Fig. 9, the current of big particles show deviations between MF and MC for intermediate densities ρ_1. On the

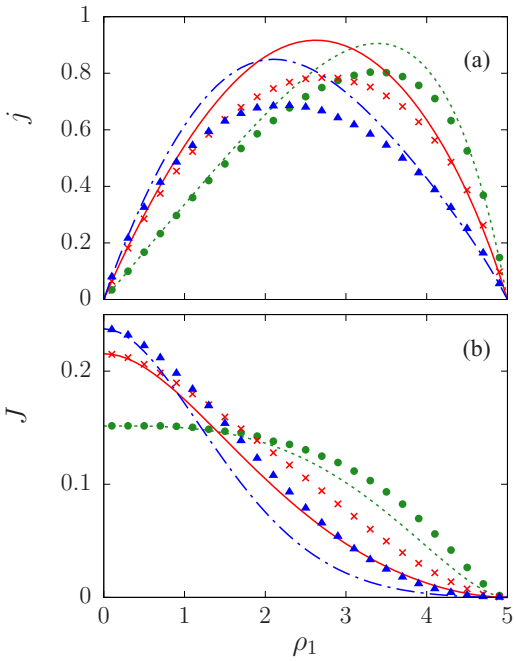

FIG. 9. Current of small particles (a) and big particles (b) for the generalized ASEP with pockets. The density of big particles is $\rho_2 = 0.5$. The rates are $a = 1$, $A = 0.5$, $b = B = 0$, $d = 0.5$, $D = 0.25$, $\gamma = \Gamma = 0.5$ (×, solid line), $\gamma = \Gamma = 2$ (•, dotted line), $\gamma = \Gamma = 0.2$ (▲, dot-dashed line).

contrary, in the regime $\rho_2 > 1$, shown in Fig. 10, the MC and MF results coincide nearly exactly. At the same time, when we compare the curves for different values of the parameter γ,

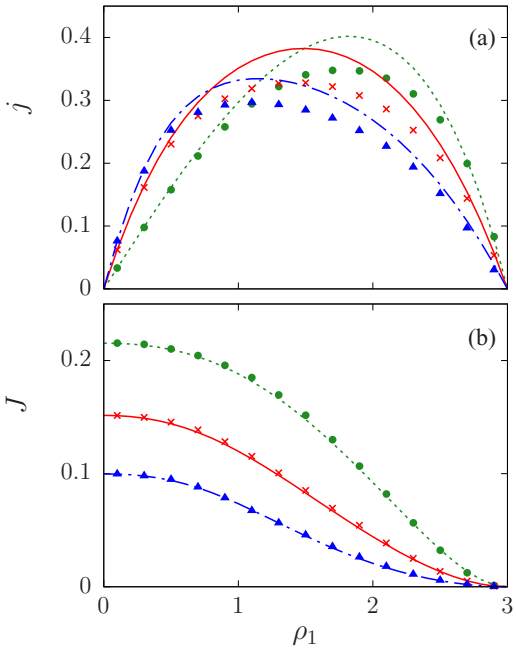

FIG. 10. Current of small particles (a) and big particles (b) for the generalized ASEP with pockets. The density of big particles is $\rho_2 = 1.5$. The rates are $a = 1$, $A = 0.5$, $b = B = 0$, $d = 0.5$, $D = 0.25$, $\gamma = \Gamma = 0.5$ (×, solid line), $\gamma = \Gamma = 2$ (•, dotted line), $\gamma = \Gamma = 0.2$ (▲, dot-dashed line).

we can see that in the $\rho_2 > 1$ regime the current of big particles always increases with increasing γ, while in the $\rho_2 < 1$ regime J increases with γ only for large ρ_1, but decreases with γ for small ρ_1. This can be understood as follows. For $\rho_2 < 1$ and few small particles, increasing γ means that more big particles are trapped in the pockets and less of them are available for movement along the backbone. When the density of small particles increase, the pockets are filled by the small particles instead, pushing the big particles out, thus increasing the number of big particles on the backbone. This causes the increase of the current of big particles. For $\rho_2 > 1$ we do not see the change of trend when increasing the density of small particles. In this case the backbone is in large part filled by big particles, thus blocking the movement of each other. Increasing γ means more big particles trapped in the pockets, which has the effect of increasing the current of big particles, rather than decreasing it. Presence of small particles does not change this behavior qualitatively. Small particles cause only overall decrease of the current due to less space to move.

As for the current of small particles, in both Figs. 9 and 10 we can see that the maximum of current is shifted to low concentrations ρ_1 at low values of γ and to high concentrations for high values of γ. This is the basis for the ratchet effect investigated in the next section.

V. SEPARATION OF PARTICLES

A. Ratchet effect

Up to now we were concerned with time-independent driving of particles and we computed only the stationary state. If we want to investigate the ratchet effect, we need to include the nonstationarity, at least on an approximate level. Here we shall use adiabatic approximation. Generically, ratchet effect occurs everywhere two conditions are satisfied, namely time-dependent driving and mirror-asymmetric geometry. However, it is not obvious a priori, if, in a specific situation, the ratchet effect is quantitatively significant or negligible. In our case, the ratchet effect occurs by a simple mechanism tightly related to the presence of pockets. We imagine that the driving is due to an external field, e.g., an electrical one, if the particles carry electrostatic charge. The pockets are dead ends tilted with respect to the axis of the backbone. Let us look at what happens in low-density regime. In an alternating external field, particles are pushed toward the dead ends in one half-period, thus emptying the backbone. This implies decreasing the current. In the next half-period of the driving, particles are pulled from the dead ends, average density on the backbone increases. Therefore, current averaged over entire period of the driving is rectified. An important point is that in the high-density regime the effect of filling and emptying the pockets has opposite consequences. Indeed, in the high-density regime, when we decrease the density at the backbone, the current increases. Therefore, we expect that not just the magnitude but even the sign of the ratchet effect depends strongly on the density of particles.

If we consider time-dependent driving in adiabatic approximation, we can use the results obtained for stationary state virtually unchanged. Specifically, we suppose that driving depends on time periodically in a stepwise manner. In the first

half of the period, we assume parameters of the model are a, b, A, B, c, d, C, and D. We also assume $a > b$ and $A > B$, i.e., in the first half period the drift is oriented rightward. In the second half of the period we exchange the values of the parameters as $a \leftrightarrow b$, $A \leftrightarrow B$, $c \leftrightarrow d$, and $C \leftrightarrow D$. A physical interpretation of such change is the following. We suppose that the particles are driven by a homogeneous external field. For example, colloid particles can carry electrostatic charge and the whole apparatus can be inserted in homogeneous but time-dependent electric field. When the orientation of the field is reversed, it corresponds to exchange the right- and left-hand side in the model. This implies the exchanges $a \leftrightarrow b$ and $A \leftrightarrow B$. As we already hinted, pockets are considered as tilted dead ends of the channel in which the colloid particles move. The rates for entering and leaving the pocket depend on the field in analogous manner as the rates for leftward and rightward jumps. Moreover, they depend on the inclination of the dead end with respect to the main channel. Inverting the orientation of the field is equivalent to inverting the inclination. This implies the exchanges $c \leftrightarrow d$, and $C \leftrightarrow D$.

We suppose that the frequency of the alternation of the external driving is so low that during each half-period the system is in a stationary state almost all the time. This is the adiabatic approximation. The quantities averaged over many time periods then can be calculated as average of stationary states with one orientation of the driving and with the opposite orientation of the driving. Particle current averaged in such a way is the ratchet current. It can be nonzero even though if we averaged the driving itself, we would get zero. The source of the ratchet current is the mirror asymmetry of the geometry in which the particles move.

For $\gamma = c/d < 1$ and $\Gamma = C/D < 1$ pockets are inclined against the direction of the driving. The pockets are emptied and the density of particles at the backbone is increased. On the other hand, for $\gamma > 1$, $\Gamma > 1$, i.e., pockets inclined along the direction of the driving, the pockets are packed with particles and the density of particles at the backbone is decreased. In the first and in the second half-periods of the periodic driving the density at the backbone is different, which results in a net ratchet current.

If the rates satisfy (44), the currents of small and big particles are proportional to $a - b$ and $A - B$, respectively. Therefore, we define quantities $\bar{j}(\gamma, \Gamma) = j/(a - b)$ and $\bar{J}(\gamma, \Gamma) = J/(A - B)$, which depend on the parameters of the model only through the fractions $\gamma = c/d$ and $\Gamma = C/D$, as indicated by the arguments. Then the ratchet currents of small and big particles in the adiabatic approximation are

$$j_{\mathrm{rat}} = \frac{a-b}{2}[\bar{j}(\gamma,\Gamma) - \bar{j}(\gamma^{-1},\Gamma^{-1})],$$
$$J_{\mathrm{rat}} = \frac{A-B}{2}[\bar{J}(\gamma,\Gamma) - \bar{J}(\gamma^{-1},\Gamma^{-1})]. \qquad (60)$$

We show the ratchet currents as functions of the density of small particles in Figs. 11–13. In all cases we have $a - b$ as well as $A - B$ positive and $\gamma < 1$, i.e., in the first half-period of the periodic driving the drift is oriented rightwards and jumps from the pocket have higher probability than to the pocket. This means that the pockets are tilted to the left, just as depicted in Fig. 1(b).

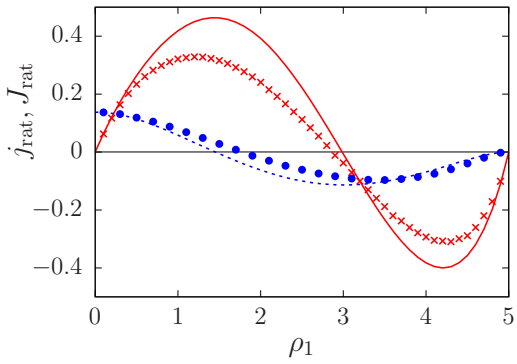

FIG. 11. Ratchet current of small particles (×, solid line), and big particles (•, dotted line). The rates are $a = A = 1$, $b = B = 0$, $d = 0.5$, $D = 0.25$, $\gamma = 0.2$. The density of big particles is $\rho_2 = 0.5$.

In all three figures we can see the typical behavior of the ratchet current of small particles. For small ρ_1 it increases, for ρ_1 increasing it achieves a maximum, and then descends to zero at some intermediate density, and beyond this point it becomes negative. Its absolute value increases again, achieves a maximum, and decreases finally to zero at a maximum allowed density. This type of dependence can be easily understood from Figs. 9 and 10. As we already stressed, the maximum of the current is at lower densities if $\gamma < 1$ and at higher densities if $\gamma > 1$. Therefore, the positive current in the first half-period dominates at lower densities, while the negative current at the second half-period dominates at higher densities. In simple words, at the second-half period, when $\gamma > 1$, particles are more accumulated in the pockets than in the first half-period. Such accumulation leads to decrease of the current for small densities, but, on the contrary, to increase of the current for higher densities.

Comparing the MC and MF results, we can see in all cases that mean-field approximation overestimates the ratchet current. This implies that correlations hinder the ratchet effect.

B. Regime of full separation

In Figs. 11–13 we can see features which play a central role in separation of particles by size. The ratchet currents of big and small particles have quite different

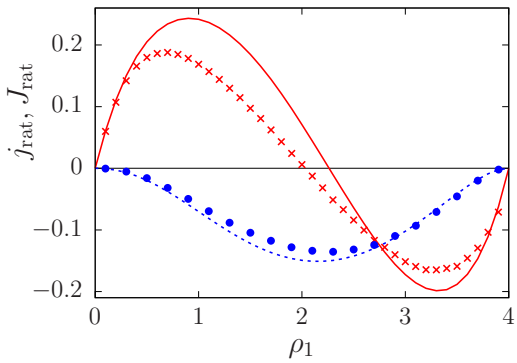

FIG. 12. Ratchet current of small particles (×, solid line), and big particles (•, dotted line). The rates are $a = A = 1$, $b = B = 0$, $d = 0.5$, $D = 0.25$, $\gamma = 0.2$. The density of big particles is $\rho_2 = 1.0$.

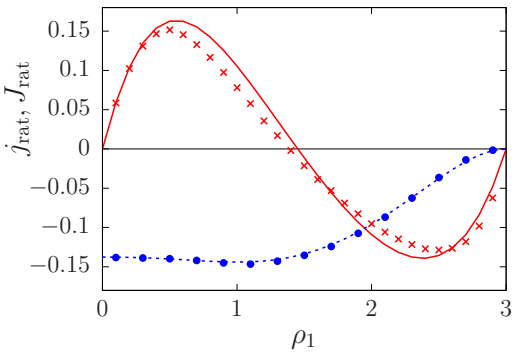

FIG. 13. Ratchet current of small particles (×, solid line), and big particles (•, dotted line). The rates are $a = A = 1$, $b = B = 0$, $d = 0.5, D = 0.25, \gamma = 0.2$. The density of big particles is $\rho_2 = 1.5$.

magnitude, and most importantly, they can have even different sign. It is the latter regime that is the most important, because this implies in principle a total separation of these particle species. In practice, however, such full separation regime can be only transitory, because it occurs only in specific region of particle densities. The separation process itself results in change of the concentrations, and in general can push the system out of the regime of full separation, unless a special trajectory in the density plane (ρ_1 vs ρ_2) is maintained.

More specifically, in Figs. 11–13 we can see that for fixed ρ_2 there is a specific interval of densities ρ_1 for which $j_{\rm rat}$ and $J_{\rm rat}$ have different sign. In Fig. 13 we can observe that for $\rho_2 = 1.5$ such interval is about $\rho_1 \in [0, 1.4]$, while for $\rho_2 = 0.5$ it is about $\rho_1 \in [1.5, 3]$. We found that in general for $\rho_2 > 1$ the interval for ρ_1 extends down to 0, while for $\rho_2 < 1$ it has positive lower limit.

The set of these intervals sums up in a phase diagram as shown in Fig. 14. We can compare the area of full separation obtained by MC simulations (shaded areas) with MF results (delimited by lines). The general feature of this diagram is that full separation occur at "diagonal" densities, i.e., at low density of small particles, if the density of big particles is large, and at low densities of big particles, if density of small particles is large, as well as at the intermediate regime, where both densities are somewhere in the middle of their allowed range.

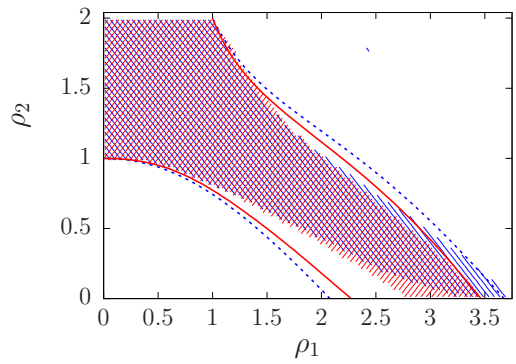

FIG. 14. Phase diagram of the ratchet separator. We indicate the area of densities for which the ratchet currents of small and big particles have opposite sign. The shaded regions are obtained by Monte Carlo simulations, the lines correspond to the mean-field approximation. The values of the parameters are $a = 1$, $A = 0.5$, $b = B = 0$, $d = 0.5$, $D = 0.25$, $\gamma = 0.1$ (area shaded as "//," solid line) and $\gamma = 0.5$ (area shaded as "\\," dotted line)

Comparing the MC and MF results, we can see that they agree very well at the part of the diagram which corresponds to high concentration of big particles, but differences are rather large in the part corresponding to low concentration of big particles. This is consistent with the generic finding we already discussed before, that addition of small number of large particles into moderately dense ensemble of small particles drastically increases correlations. This is then reflected in large difference between the MF and MC results.

VI. CONCLUSIONS

We introduced generalizations of the asymmetric simple exclusion process. The basic assumptions of ASEP are maintained. Namely, the model is endowed with stochastic dynamics; the system is discrete, i.e., it is composed of cells among which the particles jump; the system is driven, which results in nonzero current in stationary state; the particles interact by steric repulsion, i.e., there is an exclusion condition.

We generalized the standard ASEP in three directions. The first one consisted in allowing several particles sharing the same cell at the same time. This is the most important change from the standard ASEP, because it makes the model nonintegrable in general. The second generalization introduced several species of particles, each species being characterized by a specific particle size. The exclusion condition then requires that sum of sizes of all particles at the same cell does not exceed a constant k which we call capacity. The third generalization consisted in changed geometry. Instead of a linear chain of cells used in ASEP, we used an asymmetric comblike topology, in which a new cell, called a pocket, is attached to each cell on the chain.

The main question we posed was, how much this setup can serve as a model of particle separation in narrow channels. Therefore, the main quantities of interest were the currents of small and big particles. The approaches to the model were first direct Monte Carlo (MC) simulations, which were done in parallel with generalized mean-field (MF) approximation. We also found a specific case in which exact solution is possible for the stationary state.

We used the difference between MC and MF results as a qualitative measure of correlations induced by particle interaction. Generically, we found that correlations are significant in the regime of intermediate densities, but they are small in either of the limits of very small and close to maximum density of particles. An important exception is the regime of intermediate to large density of small particles, where adding even a few big particles increases the correlations significantly. It can be understood intuitively as blocking large number of small particles behind a single big particle.

The presence of pockets is essential for the ratchet effect. Ratchet effect is achieved here by making the driving time-dependent. More precisely, by periodical change of the direction of the driving, so that the driving is zero on average. In the first half-period the driving is constant and oriented rightward, in the second half-period the absolute value of the

driving is unchanged but orientation is reversed. In presence of pockets, the ratio γ of the jump rates to and from the pocket is $\gamma < 1$ in one half-period while $\gamma > 1$ in the next half-period. This results in a nonzero net current when averaged over the whole period. This is the intuitive explanation of the current rectification.

We calculated the ratchet effect in the adiabatic approximation, i.e., we assumed that the period of the driving goes to infinity. We found that the generic dependence of the ratchet current on the density of particles shows current reversal at an intermediate density of particles. The most practical finding is that the density at which the current reversal occurs, is not the same for the big and the small particles. Therefore, there is an interval of densities for which the directions of the ratchet currents of the small and big particles are opposite. In this regime, full separation of the small particles from the big ones is expected. Interestingly, in the density-density plane, the area of full separation extends "diagonally" from the states of high density of big and low density of small to the states of high density of small and low density of big.

If we imagine separation of a real mixture of colloid particles, the actual densities of both small and big particles change during the separation process. Therefore, we move in the density-density plane along a trajectory, whose shape depends on the details of the separation setup. If we are clever enough to devise the apparatus so that the trajectory goes within the "diagonal" area of full separation, we may actually end with having all big particles on one side and all small particles on the opposite side.

There are numerous directions in which we can make the model more realistic. First, the quasi-one-dimensional geometry can be enhanced by attributing a finite size to the backbone as well as to the pockets. This means that several cells can be placed one by another in transversal direction. Another important extension would be keeping finite nonzero frequency of switching the driving direction. We have made preliminary studies in a variant of the model with sinusoidally varying driving and observed strong dependence on the frequency. Moreover, at nonzero frequency, the currents show rather complicated nonlinear dependence on the strength of the driving, i.e., in our model, on the difference between rightward and leftward jump rates. These topics need more investigation, though.

ACKNOWLEDGMENTS

The work was supported by the Grant Agency of the Czech Republic, Grant No. 17-06716S. We wish to thank J. Krug, A. Schadschneider, and G. M. Schütz for numerous inspiring discussions.

APPENDIX A: MATRIX OF TRANSITION PROBABILITIES

The matrix W_2 describing the probabilities of elementary jumping transitions in Eq. (13) can be easily defined by listing all the nonzero off-diagonal elements. The list includes jumps along the backbone

$$
\begin{aligned}
W_2\left[\binom{z_1Z_1}{s_1S_1}\binom{z_2Z_2}{s_2S_2} \leftarrow \binom{z_1Z_1}{s_1+1S_1}\binom{z_2Z_2}{s_2-1S_2}\right] &= \frac{1}{\nu}(s_1+1)a\ \chi_k(s_2,S_2),\\
W_2\left[\binom{z_1Z_1}{s_1S_1}\binom{z_2Z_2}{s_2S_2} \leftarrow \binom{z_1Z_1}{s_1-1S_1}\binom{z_2Z_2}{s_2+1S_2}\right] &= \frac{1}{\nu}(s_2+1)b\ \chi_k(s_1,S_1),\\
W_2\left[\binom{z_1Z_1}{s_1S_1}\binom{z_2Z_2}{s_2S_2} \leftarrow \binom{z_1Z_1}{s_1S_1+1}\binom{z_2Z_2}{s_2S_2-1}\right] &= \frac{1}{\nu}(S_1+1)A\ \chi_k(s_2,S_2),\\
W_2\left[\binom{z_1Z_1}{s_1S_1}\binom{z_2Z_2}{s_2S_2} \leftarrow \binom{z_1Z_1}{s_1S_1-1}\binom{z_2Z_2}{s_2S_2+1}\right] &= \frac{1}{\nu}(S_2+1)B\ \chi_k(s_1,S_1),
\end{aligned}
\tag{A1}
$$

and the jumps to and from the pocket

$$
\begin{aligned}
W_2\left[\binom{z_1Z_1}{s_1S_1}\binom{z_2Z_2}{s_2S_2} \leftarrow \binom{z_1+1Z_1}{s_1-1S_1}\binom{z_2Z_2}{s_2S_2}\right] &= \frac{1}{2\nu}(z_1+1)d\ \chi_k(s_1,S_1),\\
W_2\left[\binom{z_1Z_1}{s_1S_1}\binom{z_2Z_2}{s_2S_2} \leftarrow \binom{z_1Z_1}{s_1S_1}\binom{z_2+1Z_2}{s_2-1S_2}\right] &= \frac{1}{2\nu}(z_2+1)d\ \chi_k(s_2,S_2),\\
W_2\left[\binom{z_1Z_1}{s_1S_1}\binom{z_2Z_2}{s_2S_2} \leftarrow \binom{z_1-1Z_1}{s_1+1S_1}\binom{z_2Z_2}{s_2S_2}\right] &= \frac{1}{2\nu}(s_1+1)c\ \chi_k(z_1,Z_1),\\
W_2\left[\binom{z_1Z_1}{s_1S_1}\binom{z_2Z_2}{s_2S_2} \leftarrow \binom{z_1Z_1}{s_1S_1}\binom{z_2-1Z_2}{s_2+1S_2}\right] &= \frac{1}{2\nu}(s_2+1)c\ \chi_k(z_2,Z_2),\\
W_2\left[\binom{z_1Z_1}{s_1S_1}\binom{z_2Z_2}{s_2S_2} \leftarrow \binom{z_1Z_1+1}{s_1S_1-1}\binom{z_2Z_2}{s_2S_2}\right] &= \frac{1}{2\nu}(Z_1+1)D\ \chi_k(s_1,S_1),
\end{aligned}
$$

$$W_2\left[\binom{z_1Z_1}{s_1S_1}\binom{z_2Z_2}{s_2S_2} \leftarrow \binom{z_1Z_1}{s_1S_1}\binom{z_2Z_2+1}{s_2S_2-1}\right] = \frac{1}{2\nu}(Z_2+1)D\ \chi_k(s_2,S_2),$$
$$W_2\left[\binom{z_1Z_1}{s_1S_1}\binom{z_2Z_2}{s_2S_2} \leftarrow \binom{z_1Z_1-1}{s_1S_1+1}\binom{z_2Z_2}{s_2S_2}\right] = \frac{1}{2\nu}(S_1+1)C\ \chi_k(z_1,Z_1),$$
$$W_2\left[\binom{z_1Z_1}{s_1S_1}\binom{z_2Z_2}{s_2S_2} \leftarrow \binom{z_1Z_1}{s_1S_1}\binom{z_2Z_2-1}{s_2S_2+1}\right] = \frac{1}{2\nu}(S_2+1)C\ \chi_k(z_2,Z_2). \tag{A2}$$

APPENDIX B: TWO-SPECIES GENERALIZED ASEP

1. Construction of the master equation

The right-hand side of the analog of Eq. (17) includes also contributions from jumps of big particles, $X_{\rm L}$ and $X_{\rm R}$:

$$\frac{d}{dt}P^{(1)}_{sS} = x_{\rm L} + x_{\rm R} + X_{\rm L} + X_{\rm R}, \tag{B1}$$

where $X_{\rm L} = X^-_{\rm L} + X^+_{\rm L}$ and $X_{\rm R} = X^-_{\rm R} + X^+_{\rm R}$. Explicit expressions for all the terms read

$$\begin{aligned}
x^-_{\rm L} &= -b_s l^{\rm L}_{sS} - \tilde\delta_{s+2S,k} u^{\rm L}_{sS},\\
x^+_{\rm L} &= \tilde\delta_{s+2S,k} b_{s+1} l^{\rm L}_{s+1,S} + \tilde\delta_{s,0} u^{\rm L}_{s-1,S},\\
x^-_{\rm R} &= -a_s l^{\rm R}_{sS} - \tilde\delta_{s+2S,k} u^{\rm R}_{sS},\\
x^+_{\rm R} &= \tilde\delta_{s+2S,k} a_{s+1} l^{\rm R}_{s+1,S} + \tilde\delta_{s,0} u^{\rm R}_{s-1,S}
\end{aligned} \tag{B2}$$

for small particles and

$$\begin{aligned}
X^-_{\rm L} &= -B_S L^{\rm L}_{sS} - \tilde{\tilde\delta}_{s+2S,k} U^{\rm L}_{sS},\\
X^+_{\rm L} &= \tilde{\tilde\delta}_{s+2S,k} B_{S+1} L^{\rm L}_{s,S+1} + \tilde\delta_{S,0} U^{\rm L}_{s,S-1},\\
X^-_{\rm R} &= -A_S L^{\rm R}_{sS} - \tilde{\tilde\delta}_{s+2S,k} U^{\rm R}_{sS},\\
X^+_{\rm R} &= \tilde{\tilde\delta}_{s+2S,k} A_{S+1} L^{\rm R}_{s,S+1} + \tilde\delta_{S,0} U^{\rm R}_{s,S-1}
\end{aligned} \tag{B3}$$

for big particles, where $\tilde{\tilde\delta}_{s+2S,k} = 1 - \delta_{s+2S,k} - \delta_{s+2S,k-1}$ stands for highly occupied states in the case of jumps of big particles. Four states $(s-1,S)$, $(s+1,S)$ and $(s,S-1)$, $(s,S+1)$ contribute to the gain terms. The selective functions l, u and L, U are defined as follows:

$$\begin{aligned}
l^{\rm L}_{sS} &= \sum_{s',S'}^{(k-1)} P^{(2)}_{s'S';sS}, \quad u^{\rm L}_{sS} = \sum_{s',S'}^{(k)} a_{s'} P^{(2)}_{s'S';sS},\\
l^{\rm R}_{sS} &= \sum_{s',S'}^{(k-1)} P^{(2)}_{sS;s'S'}, \quad u^{\rm R}_{sS} = \sum_{s',S'}^{(k)} b_{s'} P^{(2)}_{sS;s'S'},\\
L^{\rm L}_{sS} &= \sum_{s',S'}^{(k-2)} P^{(2)}_{s'S';sS}, \quad U^{\rm L}_{sS} = \sum_{s',S'}^{(k)} A_{S'} P^{(2)}_{s'S';sS},\\
L^{\rm R}_{sS} &= \sum_{s',S'}^{(k-2)} P^{(2)}_{sS;s'S'}, \quad U^{\rm R}_{sS} = \sum_{s',S'}^{(k)} B_{S'} P^{(2)}_{sS;s'S'},
\end{aligned} \tag{B4}$$

where the upper limit of the sum given in parentheses, like $\sum^{(m)}_{s,S}$, has the meaning that the summation is carried over all non-negative integers s and S satisfying the condition $s + 2S \leqslant m$.

The currents of small and big particles read

$$j = \sum_{s,S}^{(k)} \sum_{s',S'}^{(k-1)} a_s P^{(2)}_{sS;s'S'} - \sum_{s,S}^{(k-1)} \sum_{s',S'}^{(k)} b_{s'} P^{(2)}_{sS;s'S'}, \tag{B5}$$

$$J = \sum_{s,S}^{(k)} \sum_{s',S'}^{(k-2)} A_S P^{(2)}_{sS;s'S'} - \sum_{s,S}^{(k-2)} \sum_{s',S'}^{(k)} B_{S'} P^{(2)}_{sS;s'S'}\ . \tag{B6}$$

Under periodic boundary conditions, the mean-field approximation $P^{(2)}_{sS;s'S'} \approx P^{(1)}_{sS} P^{(1)}_{s'S'}$ makes the selective functions to simplify

$$l^{\rm L}_{sS} = l^{\rm R}_{sS} = P^{(1)}_{sS} l, \quad u^{\rm L}_{sS} = P^{(1)}_{sS} u_a, \quad u^{\rm R}_{sS} = P^{(1)}_{sS} u_b, \tag{B7}$$

where

$$l = \sum_{s',S'}^{(k-1)} P^{(1)}_{s'S'}, \quad u_a = \sum_{s',S'}^{(k)} a_{s'} P^{(1)}_{s'S'}, \quad u_b = \sum_{s',S'}^{(k)} b_{s'} P^{(1)}_{s'S'} \tag{B8}$$

and

$$L^{\rm L}_{sS} = L^{\rm R}_{sS} = P^{(1)}_{sS} L, \quad U^{\rm L}_{sS} = P^{(1)}_{sS} U_A, \quad U^{\rm R}_{sS} = P^{(1)}_{sS} U_B \tag{B9}$$

with

$$L = \sum_{s',S'}^{(k-2)} P^{(1)}_{s'S'}, \quad U_A = \sum_{s',S'}^{(k)} A_{S'} P^{(1)}_{s'S'}, \quad U_B = \sum_{s',S'}^{(k)} B_{S'} P^{(1)}_{s'S'}. \tag{B10}$$

2. Reduction to single equation for $k = 3$

We start from the master equations (39). Two quasilinear relations follow from the equation for P_{30} and its combination with that for P_{20}: $P_{10} = \phi h_2 P_{20}$ and $P_{20} = \phi h_3 P_{30}$, where $\phi = l/u$. Adding the equations for P_{00} and P_{01} yields one more relation:

$$P_{00} + P_{01} = \phi h_1 (P_{10} + P_{11}). \tag{B11}$$

Another type of a relation is deduced if we add the equations for P_{01} and P_{11}:

$$P_{00} + P_{10} = \Phi H_1 (P_{01} + P_{11}) \tag{B12}$$

with $\Phi = L/U$.

Let us show that Eqs. (B11) and (B12) can be split. Using their definitions, L and U can be eliminated from the LU part, say, of the equation for P_{01} to yield

$$-H_1 P_{01} L + P_{00} U = -H_1 P_{01} P_{10} + H_1 P_{00} P_{11}. \tag{B13}$$

Then the equation for P_{01} takes the following form:

$$\frac{(1/h_1)P_{01}}{P_{11}} = \frac{H_1/h_1 P_{00} + l}{H_1 P_{10} + u}. \tag{B14}$$

The numerator and denominator of the left-hand side of this proportion multiplied by H_1 are added to those of the right-hand side [93] resulting in

$$\frac{P_{01}}{h_1 P_{11}} = \frac{H_1/h_1 P_{00} + l + H_1/h_1 P_{01}}{H_1 P_{10} + u + H_1 P_{11}}. \tag{B15}$$

Next, the equation for P_{00} is transformed making use of relation (B13) to the following:

$$\frac{(1/h_1)P_{00}}{P_{10}} = \frac{l + H_1/h_1 P_{01}}{u + H_1 P_{11}}. \tag{B16}$$

Owing to the same property of a proportion [93], fraction $(1/h_1)P_{00}/P_{10}$ appears to equal the right-hand side of Eq. (B15) resulting in $P_{00}/(h_1 P_{10}) = P_{01}/(h_1 P_{11})$. Equation (B11) shows now that these fractions are equal to ϕ or $P_{00} = \phi h_1 P_{10}$ and $P_{01} = \phi h_1 P_{11}$. These relations rewritten as $h_1 P_{10} l - P_{00} u = 0$ and $h_1 P_{11} l - P_{01} u = 0$ immediately split the lu and LU parts in the corresponding master equations. Then

$$H_1 P_{01} L - P_{00} U = 0, \quad H_1 P_{11} L - P_{10} U = 0, \tag{B17}$$

i.e., $P_{00} = \Phi H_1 P_{01}$ and $P_{10} = \Phi H_1 P_{11}$ splitting Eq. (B12).

Now, we derive an equation for ϕ. The normalization condition is multiplied by ρ_1 and ρ_2 and subtracted from ρ_1- and ρ_2-fixing conditions (35) to yield

$$\sum_{s,S}^{(k)} P_{sS}\,(\rho_1 - s) = 0, \quad \sum_{s,S}^{(k)} P_{sS}\,(\rho_2 - S) = 0. \tag{B18}$$

All the probabilities are expressed through P_{30} as

$$\begin{aligned} P_{00} &= \phi^3 h_1 h_2 h_3 P_{30}, \\ P_{10} &= \phi^2 h_2 h_3 P_{30}, \\ P_{20} &= \phi h_3 P_{30}, \\ P_{01} &= \frac{\phi^3 h_1 h_2 h_3}{\Phi H_1} P_{30}, \\ P_{11} &= \frac{\phi^2 h_2 h_3}{\Phi H_1} P_{30} \end{aligned} \tag{B19}$$

and inserted into Eqs. (B18) resulting in a closed set for ϕ and Φ:

$$\begin{aligned} &\rho_1\phi^3 + \frac{\rho_1 - 1}{h_1}\phi^2 + \frac{\rho_1 - 2}{h_1 h_2}\phi + \frac{\rho_1 - 3}{h_1 h_2 h_3} \\ &\quad + \frac{\phi^2}{H_1\Phi}\left[\rho_1\phi + \frac{\rho_1 - 1}{h_1}\right] = 0, \\ &\rho_2\left(\phi^3 + \frac{1}{h_1}\phi^2 + \frac{1}{h_1 h_2}\phi + \frac{1}{h_1 h_2 h_3}\right) \\ &\quad + \frac{\phi^2}{H_1\Phi}(\rho_2 - 1)\left[\phi + \frac{1}{h_1}\right] = 0. \end{aligned} \tag{B20}$$

When we eliminate Φ from these equations, we obtain a single equation for ϕ, which is Eq. (41).

Having obtained the solution in terms of ϕ, we need to reconstruct the probabilities. P_{11} can be written in terms of ϕ using $P_{01} = \phi h_1 P_{11}$ and the ρ_2-fixing condition as $P_{11} = \rho_2/(1 + h_1\phi)$. Hence

$$P_{01} = \frac{\rho_2 h_1 \phi}{1 + h_1\phi}. \tag{B21}$$

Remaining probabilities are computed using relations (B19). Since all P_{sS} are now expressed through ϕ, and $H_1 = (A_1 + B_1)/(a + b)$ does not enter the final equation for ϕ, it follows that the steady-state probabilities do not depend on the jump rates of big particles, A_1 and B_1.

APPENDIX C: ONE-SPECIES GENERALIZED ASEP WITH POCKETS

1. Master equation

In case on the chain composed of a backbone and pockets attached to each backbone cell, the equation for one-site probability $P^{(1)}_{sz}$ can be written as

$$\frac{d}{dt}P^{(1)}_{sz} = x_{\mathrm{L}} + x_{\mathrm{R}} + y, \tag{C1}$$

where $x_{\mathrm{L}} = x^-_{\mathrm{L}} + x^+_{\mathrm{L}}$, $x_{\mathrm{R}} = x^-_{\mathrm{R}} + x^+_{\mathrm{R}}$, while $y = y^- + y^+$ describes one-site processes involving jumps to and from the pocket. We again write these terms through selective functions l and u which are now specified for each pair (s, z):

$$\begin{aligned} x^-_{\mathrm{L}} &= -b_s l^{\mathrm{L}}_{sz} - \tilde{\delta}_{s,k} u^{\mathrm{L}}_{sz}, \\ x^+_{\mathrm{L}} &= \tilde{\delta}_{s,k} b_{s+1} l^{\mathrm{L}}_{s+1,z} + \tilde{\delta}_{s,0} u^{\mathrm{L}}_{s-1,z}, \\ x^-_{\mathrm{R}} &= -a_s l^{\mathrm{R}}_{sz} - \tilde{\delta}_{s,k} u^{\mathrm{R}}_{sz}, \\ x^+_{\mathrm{R}} &= \tilde{\delta}_{s,k} a_{s+1} l^{\mathrm{R}}_{s+1,z} + \tilde{\delta}_{s,0} u^{\mathrm{R}}_{s-1,z}. \end{aligned} \tag{C2}$$

Expressions for the functions l and u are as follows:

$$\begin{aligned} l^{\mathrm{L}}_{sz} &= \sum_{s'=0}^{k-1} P^{(2)}_{s'+,sz}, \quad u^{\mathrm{L}}_{sz} = \sum_{s'=1}^{k} a_{s'} P^{(2)}_{s'+,sz}, \\ l^{\mathrm{R}}_{sz} &= \sum_{s'=0}^{k-1} P^{(2)}_{sz,s'+}, \quad u^{\mathrm{R}}_{sz} = \sum_{s'=1}^{k} b_{s'} P^{(2)}_{sz,s'+}, \end{aligned} \tag{C3}$$

where total summation is understood over the pocket index denoted by subscript "+," as in, e.g.,

$$P^{(2)}_{s'+,sz} = \sum_{z'=0}^{k} P^{(2)}_{s'z',sz} \tag{C4}$$

since the pocket state does not influence on jumps. The loss and gain contributions,

$$\begin{aligned} y^- &= -\tilde{\delta}_{z,q} c_s P^{(1)}_{sz} - \tilde{\delta}_{s,k} d_z P^{(1)}_{sz}, \\ y^+ &= \tilde{\delta}_{s,k}\tilde{\delta}_{z,0} c_{s+1} P^{(1)}_{s+1,z-1} + \tilde{\delta}_{z,q}\tilde{\delta}_{s,0} d_{z+1} P^{(1)}_{s-1,z+1}, \end{aligned} \tag{C5}$$

describe entering and leaving the pocket being in state s, z (direct processes) and their inverses, respectively; $\tilde{\delta}$'s come to play for fully occupied and empty pocket or site.

The current between two neighboring sites is defined by

$$j = \sum_{s=1}^{k}\sum_{s'=0}^{k-1} a_s P^{(2)}_{s+,s'+} - \sum_{s=0}^{k-1}\sum_{s'=1}^{k} b_{s'} P^{(2)}_{s+,s'+} \tag{C6}$$

with total summations taken over the pocket indices denoted by "+," as before.

In the mean-field approximation we neglect correlations between sites, $P^{(2)}_{sz,s'z'} \approx P^{(1)}_{sz} P^{(1)}_{s'z'}$. In this approximation, the selective functions are $l^{\mathrm{L}}_{sz} = l^{\mathrm{R}}_{sz} \approx P^{(1)}_{sz} l$, $u^{\mathrm{L}}_{sz} \approx P^{(1)}_{sz} u_a$, $u^{\mathrm{R}}_{sz} \approx P^{(1)}_{sz} u_b$, where

$$l = \sum_{s'=0}^{k-1} P^{(1)}_{s'+}, \quad u_a = \sum_{s'=1}^{k} a_{s'} P^{(1)}_{s'+}, \quad u_b = \sum_{s'=1}^{k} b_{s'} P^{(1)}_{s'+}. \tag{C7}$$

2. Reduction to single equation for $k = 1$

When the backbone cell accepts at most one particle, the master equations read, according to Eq. (47),

$$\begin{aligned}
P_{00} &: 0 = (a+b)[h_1 P_{10} l - P_{00} u], \\
P_{10} &: 0 = (a+b)[-h_1 P_{10} l + P_{00} u] - c_1 P_{10} + d_1 P_{01}, \\
&\dots \\
P_{0z} &: 0 = (a+b)[h_1 P_{1z} l - P_{0z} u] + c_1 P_{1,z-1} - d_z P_{0z}, \\
P_{1z} &: 0 = (a+b)[-h_1 P_{1z} l + P_{0z} u] - c_1 P_{1z} + d_{z+1} P_{0,z+1}, \\
&\dots \\
P_{0q} &: 0 = (a+b)[h_1 P_{1q} l - P_{0q} u] + c_1 P_{1,q-1} - d_q P_{0q}, \\
P_{1q} &: 0 = (a+b)[-h_1 P_{1q} l + P_{0q} u],
\end{aligned} \tag{C8}$$

with the mean-field l and u defined as

$$l = \sum_{s=0}^{k-1} \sum_{z=0}^{q} P_{sz}, \quad u = \sum_{s=1}^{k} h_s \sum_{z=0}^{q} P_{sz}, \tag{C9}$$

and $h_1 = 1$. Consecutive adding splits the set (C8) into two subsets: $0 = P_{1z} l - P_{0z} u|_{z=0,1,\dots,q}$ and $0 = -c_1 P_{1z} + d_{z+1} P_{0,z+1}|_{z=0,1,\dots,q-1}$ resulting in $2q+1$ relations:

$$P_{0z} = \phi P_{1z}, \quad P_{0z} = \gamma_z P_{1,z-1}, \tag{C10}$$

where $\phi = l/u$, $\gamma_z = c_1/d_z$. We combine these equations to obtain the recurrence $P_{1,z-1} = \frac{\phi}{\gamma_z} P_{1z}$ which yields

$$P_{1z} = \frac{\phi^{q-z}}{\gamma_{z+1} \dots \gamma_q} P_{1q}, \quad P_{0z} = \frac{\phi^{q-z+1}}{\gamma_{z+1} \dots \gamma_q} P_{1q}. \tag{C11}$$

P_{1q} can be expressed in terms of ϕ by inserting these formulas into the normalization condition $\sum_{s,z} P_{sz} = 1$:

$$P_{1q} = \gamma_1 \gamma_2 \dots \gamma_q \times \left[\phi^{q+1} + \sum_{z=1}^{q} \gamma_1 \dots \gamma_{z-1} (\gamma_z + 1) \phi^{q+1-z} + \gamma_1 \dots \gamma_q \right]^{-1}. \tag{C12}$$

Now, the density-fixing condition is subtracted from the normalization condition multiplied by ρ_1 to yield

$$\sum_{s=0}^{k} \sum_{z=0}^{q} P_{sz} (\rho_1 - s - z) = 0. \tag{C13}$$

When we insert into (C13) expressions (C11) for the probabilities, we obtain the equation for ϕ:

$$\rho_1 \phi^{q+1} + \sum_{z=1}^{q} \gamma_1 \dots \gamma_{z-1} (\gamma_z + 1)(\rho_1 - z) \phi^{q+1-z} + \gamma_1 \dots \gamma_q [\rho_1 - (q+1)] = 0. \tag{C14}$$

If the rates satisfy $d_z = zd$, we have $\gamma_z = \gamma/z$ with $\gamma = c/d$ and the equation for ϕ has the form

$$\sum_{z=0}^{q} \frac{\gamma^{z-1}(\gamma + z)}{z!} (\rho_1 - z) \phi^{q+1-z} + \frac{\gamma^q}{q!} [\rho_1 - (q+1)] = 0. \tag{C15}$$

The site state and the pocket state appear to be uncorrelated. Functions l and u in the case $k = 1$ are reduced to $P_{0+} = \sum_{z'=0}^{q} P_{0z'}$ and $P_{1+} = \sum_{z'=0}^{q} P_{1z'}$ (with $h_1 = 1$.) Thus, relation $P_{0z}/P_{1z} = l/u$ can be rewritten as $P_{0z} P_{1+} = P_{1z} P_{0+}$. The normalization condition in the form $P_{0+} = 1 - P_{1+}$ is substituted into the right-hand side to yield $P_{1z} = P_{1+} P_{+z}$, where $P_{+z} = P_{0z} + P_{1z}$. This result exactly means no correlation between site state $s = 1$ and arbitrary pocket state z. The case $s = 0$ is similar, and we obtain $P_{sz} = P_{s+} P_{+z}$.

3. Reduction to single equation for $k \geqslant 2$

Numerical study of the model with $k = 2$ and $q = 1$ shows that the solution to the master equations in the special case $h_1 = 1, h_2 = 2$ and $c_1 = c, c_2 = 2c$ are such that the jump and pocket parts of each equation equals zero separately. In other words, each master equation splits onto zero-value jump and pocket parts. Numerical calculations for the model with $k = 2$ and $q = 2$ with occupancy-proportional rates show the same feature.

Within the assumption of such splitting, two sets of relations can be derived from Eq. (47):

$$\begin{aligned}
P_{0z} &= \phi h_1 P_{1z}, \\
P_{1z} &= \phi h_2 P_{2z}, \\
&\dots \\
P_{k-1,z} &= \phi h_k P_{kz},
\end{aligned} \tag{C16}$$

with $z = 0, 1, \dots, q$, and

$$\begin{aligned}
\gamma_{1,z+1} P_{1z} &= P_{0,z+1}, \\
\gamma_{2,z+1} P_{2z} &= P_{1,z+1}, \\
&\dots \\
\gamma_{k,z+1} P_{kz} &= P_{k-1,z+1},
\end{aligned} \tag{C17}$$

with $z = 0, 1, \dots, q-1$ and $\gamma_{s,z+1} = c_s/d_{z+1}$. We require that these relations do not contradict each other. For example, P_{21} can be expressed through P_{22} in two ways: using the relation with P_{31}, to yield $P_{21} = \phi h_3 P_{22}/\gamma_{32}$ and alternatively by the relation to P_{12} which reads: $P_{21} = \phi h_2 P_{22}/\gamma_{22}$. These two expressions are not contradictory if $h_3/\gamma_{32} = h_2/\gamma_{22}$ or $h_3/c_3 = h_2/c_2$. The general form of the conditions of consistency reads

$$\frac{h_{s+1}}{c_{s+1}} = \frac{h_s}{c_s}, \quad s = 1, 2, \dots, k-1. \tag{C18}$$

If the rates a_s, b_s, and c_s are proportional to s, these requirements are satisfied.

The two sets of relations (C16) and (C17) can be used to express all the probabilities through P_{kq} as

$$P_{sz} = w_{sz} P_{kq}. \tag{C19}$$

This expression is inserted into the normalization condition resulting in

$$P_{kq} = \left[\sum_{s,z=0}^{k,q} w_{sz}\right]^{-1}. \tag{C20}$$

Let us obtain w_{sz}. Using relation $P_{sz} = \phi h_{s+1} P_{s+1,z}$ repeatedly we get

$$P_{sz} = \phi^{k-s} h_{s+1} h_{s+2} \cdots h_k P_{kz}. \tag{C21}$$

P_{kz} can be related to P_{kq} by repeated application of the recurrence relation $P_{kz} = \phi h_k P_{k,z+1}/\gamma_{k,z+1}$, which gives

$$P_{kz} = \frac{(\phi h_k)^{q-z}}{\gamma_{k,z+1}\gamma_{k,z+2}\cdots\gamma_{kq}} P_{kq}. \tag{C22}$$

Substitution of this expression into Eq. (C21) yields

$$w_{sz} = \frac{h_{s+1}h_{s+2}\cdots h_k\, h_k^{q-z}}{\gamma_{k,z+1}\gamma_{k,z+2}\cdots\gamma_{kq}} \phi^{k+q-s-z}. \tag{C23}$$

We derive the equation for ϕ from relation

$$\sum_{s,z=0}^{k,q} w_{sz}(\rho_1 - s - z) = 0 \tag{C24}$$

obtained by insertion of Eqs. (C19) into the difference of the normalization condition multiplied by ρ_1 and the ρ_1-fixing condition. Combination of this relation with Eq. (C23) produces the following equation:

$$\sum_{s=0}^{k}\sum_{z=0}^{q} \frac{\gamma_{k1}\gamma_{k2}\cdots\gamma_{kz}}{h_1 h_2 \cdots h_s\, h_k^z} \phi^{k+q-s-z}(\rho_1 - s - z) = 0. \tag{C25}$$

All $\{h\}$ are included here. Regarding the pocket rates, only combinations $\gamma_{kz} = c_k/d_z$ are present, whereas other c_s are not involved owing to conditions (C18). For $k = q = 3$, Eq. (C25) has the form

$$\begin{aligned}
&\rho_1\phi^6 + \frac{1}{h_1}\left(1 + \gamma_{31}\frac{h_1}{h_3}\right)(\rho_1 - 1)\phi^5 \\
&+ \frac{1}{h_1 h_2}\left(1 + \gamma_{31}\frac{h_2}{h_3} + \gamma_{31}\gamma_{32}\frac{h_1 h_2}{h_3^2}\right)(\rho_1 - 2)\phi^4 \\
&+ \frac{1}{h_1 h_2 h_3}\left(1 + \gamma_{31} + \gamma_{31}\gamma_{32}\frac{h_2}{h_3}\right. \\
&\left.+ \gamma_{31}\gamma_{32}\gamma_{33}\frac{h_1 h_2}{h_3^2}\right)(\rho_1 - 3)\phi^3 \\
&+ \frac{\gamma_{31}}{h_1 h_2 h_3^2}\left(1 + \gamma_{32} + \gamma_{32}\gamma_{33}\frac{h_2}{h_3}\right)(\rho_1 - 4)\phi^2 \\
&+ \frac{\gamma_{31}\gamma_{32}}{h_1 h_2 h_3^3}(1 + \gamma_{33})(\rho_1 - 5)\phi \\
&+ \frac{\gamma_{31}\gamma_{32}\gamma_{33}}{h_1 h_2 h_3^4}(\rho_1 - 6) = 0.
\end{aligned} \tag{C26}$$

In the case of $h_s = s$, $c_s = sc$, and $d_z = zd$ it is reduced to Eq. (51).

APPENDIX D: TWO-SPECIES GENERALIZED ASEP WITH POCKETS

1. Master equation

We construct the master equation by combining the results for the two-species generalized ASEP and the one-species generalized ASEP with pockets, Eqs. (B1) and (C1). The master equation has the form

$$\frac{d}{dt}P^{(1)}_{sS,zZ} = x_{\rm L} + x_{\rm R} + y + X_{\rm L} + X_{\rm R} + Y. \tag{D1}$$

Each term in the right-hand side has a loss (−) and a gain (+) part. The terms corresponding to jumps along the backbone are

$$\begin{aligned}
x^-_{\rm L} &= -b_s l^{\rm L}_{sS,zZ} - \tilde\delta_{s+2S,k} u^{\rm L}_{sS,zZ}, \\
x^+_{\rm L} &= \tilde\delta_{s+2S,k} b_{s+1} l^{\rm L}_{s+1,S,zZ} + \tilde\delta_{s,0} u^{\rm L}_{s-1,S,zZ}, \\
x^-_{\rm R} &= -a_s l^{\rm R}_{sS,zZ} - \tilde\delta_{s+2S,k} u^{\rm R}_{sS,zZ}, \\
x^+_{\rm R} &= \tilde\delta_{s+2S,k} a_{s+1} l^{\rm R}_{s+1,S,zZ} + \tilde\delta_{s,0} u^{\rm R}_{s-1,S,zZ},
\end{aligned} \tag{D2}$$

and

$$\begin{aligned}
X^-_{\rm L} &= -B_S L^{\rm L}_{sS,zZ} - \tilde{\tilde\delta}_{s+2S,k} U^{\rm L}_{sS,zZ}, \\
X^+_{\rm L} &= \tilde{\tilde\delta}_{s+2S,k} B_{S+1} L^{\rm L}_{s,S+1,zZ} + \tilde\delta_{S,0} U^{\rm L}_{s,S-1,zZ}, \\
X^-_{\rm R} &= -A_S L^{\rm R}_{sS,zZ} - \tilde{\tilde\delta}_{s+2S,k} U^{\rm R}_{sS,zZ}, \\
X^+_{\rm R} &= \tilde{\tilde\delta}_{s+2S,k} A_{S+1} L^{\rm R}_{s,S+1,zZ} + \tilde\delta_{S,0} U^{\rm R}_{s,S-1,zZ}.
\end{aligned} \tag{D3}$$

The corresponding selective functions l, u and L, U read

$$\begin{aligned}
l^{\rm L}_{sS,zZ} &= \sum_{s',S'}^{(k-1)} P^{(2)}_{s'S'++;sS,zZ}, \quad u^{\rm L}_{sS,zZ} = \sum_{s',S'}^{(k)} a_{s'} P^{(2)}_{s'S'++;sS,zZ}, \\
l^{\rm R}_{sS,zZ} &= \sum_{s',S'}^{(k-1)} P^{(2)}_{sS,zZ;s'S'++}, \quad u^{\rm R}_{sS,zZ} = \sum_{s',S'}^{(k)} b_{s'} P^{(2)}_{sS,zZ;s'S'++},
\end{aligned} \tag{D4}$$

and

$$\begin{aligned}
L^{\rm L}_{sS,zZ} &= \sum_{s',S'}^{(k-2)} P^{(2)}_{s'S'++;sS,zZ}, \\
U^{\rm L}_{sS,zZ} &= \sum_{s',S'}^{(k)} A_{S'} P^{(2)}_{s'S'++;sS,zZ}, \\
L^{\rm R}_{sS,zZ} &= \sum_{s',S'}^{(k-2)} P^{(2)}_{sS,zZ;s'S'++}, \\
U^{\rm R}_{sS,zZ} &= \sum_{s',S'}^{(k)} B_{S'} P^{(2)}_{sS,zZ;s'S'++},
\end{aligned} \tag{D5}$$

where "++" in the subscripts denote total summation over pocket indices, e.g.,

$$P^{(2)}_{s'S'++;sS,zZ} = \sum_{z',Z'}^{(q)} P_{s'S',z'Z';sS,zZ} \tag{D6}$$

(and analogously in all other cases), where the upper summation limit "(q)" means that the summation is restricted by the condition $z' + 2Z' \leqslant q$. The contributions of pocket processes for small and big particles can be written as

$$\begin{aligned} y^- &= -\tilde{\delta}_{z+2Z,q} c_s P^{(1)}_{sS,zZ} - \tilde{\delta}_{s+2S,k} d_z P^{(1)}_{sS,zZ}, \\ y^+ &= \tilde{\delta}_{s+2S,k} \tilde{\delta}_{z,0} c_{s+1} P^{(1)}_{s+1,S,z-1,Z} \\ &\quad + \tilde{\delta}_{z+2Z,q} \tilde{\delta}_{s,0} d_{z+1} P^{(1)}_{s-1,S,z+1,Z}, \\ Y^- &= -\tilde{\tilde{\delta}}_{z+2Z,q} C_S P^{(1)}_{sS,zZ} - \tilde{\tilde{\delta}}_{s+2S,k} D_Z P^{(1)}_{sS,zZ}, \\ Y^+ &= \tilde{\tilde{\delta}}_{s+2S,k} \tilde{\delta}_{Z,0} C_{S+1} P^{(1)}_{s,S+1,z,Z-1} \\ &\quad + \tilde{\tilde{\delta}}_{z+2Z,q} \tilde{\delta}_{S,0} D_{Z+1} P^{(1)}_{s,S-1,z,Z+1}. \end{aligned} \tag{D7}$$

The currents of small and big particles are as follows:

$$j = \sum_{s,S}^{(k)} \sum_{s',S'}^{(k-1)} a_s P^{(2)}_{sS++;s'S'++} - \sum_{s,S}^{(k-1)} \sum_{s',S'}^{(k)} b_{s'} P^{(2)}_{sS++;s'S'++}, \tag{D8}$$

$$J = \sum_{s,S}^{(k)} \sum_{s',S'}^{(k-2)} A_S P^{(2)}_{sS++;s'S'++} - \sum_{s,S}^{(k-2)} \sum_{s',S'}^{(k)} B_{S'} P^{(2)}_{sS++;s'S'++}. \tag{D9}$$

2. Mean-field approximation

The mean-field approximation $P^{(2)}_{sS,zZ;s'S',z'Z'} \approx P^{(1)}_{sS,zZ} P^{(1)}_{s'S',z'Z'}$ within the periodic bounary conditions splits the selective functions:

$$\begin{aligned} l^{\mathrm{L}}_{sS,zZ} &= l^{\mathrm{R}}_{sS,zZ} = P^{(1)}_{sS,zZ} l, \quad u^{\mathrm{L}}_{sS,zZ} = P^{(1)}_{sS,zZ} u_a, \\ u^{\mathrm{R}}_{sS,zZ} &= P^{(1)}_{sS,zZ} u_b, \end{aligned} \tag{D10}$$

where

$$l = \sum_{s',S'}^{(k-1)} P^{(1)}_{s'S'++}, \quad u_a = \sum_{s',S'}^{(k)} a_{s'} P^{(1)}_{s'S'++}, \quad u_b = \sum_{s',S'}^{(k)} b_{s'} P^{(1)}_{s'S'++}, \tag{D11}$$

and

$$\begin{aligned} L^{\mathrm{L}}_{sS,zZ} &= L^{\mathrm{R}}_{sS,zZ} = P^{(1)}_{sS,zZ} L, \quad U^{\mathrm{L}}_{sS,zZ} = P^{(1)}_{sS,zZ} U_A, \\ U^{\mathrm{R}}_{sS,zZ} &= P^{(1)}_{sS,zZ} U_B, \end{aligned} \tag{D12}$$

with

$$L = \sum_{s',S'}^{(k-2)} P^{(1)}_{s'S'++},$$

$$U_A = \sum_{s',S'}^{(k)} A_{S'} P^{(1)}_{s'S'++}, \quad U_B = \sum_{s',S'}^{(k)} B_{S'} P^{(1)}_{s'S'++}. \tag{D13}$$

In the case $k = q = 3$ explicit expressions for functions l, L and u, U defined in (55) read

$$\begin{aligned} l &= P_{00,++} + P_{10,++} + P_{20,++} + P_{01,++}, \\ u &= h_1 P_{10,++} + h_2 P_{20,++} + h_3 P_{30,++} + h_1 P_{11,++}, \\ L &= P_{00,++} + P_{10,++}, \\ U &= H_1 P_{01,++} + H_1 P_{11,++}. \end{aligned} \tag{D14}$$

If the rates are proportional to occupancies, the set of stationary master equations can be reduced to two equations for $\phi = l/u$ and $\psi = U/L$ in the way discussed in Appendix C 3. This way we get the pair of equations (58) and (59).

[1] P. Huber, J. Phys.: Condens. Matter **27**, 103102 (2015).
[2] C. Bechinger, R. Di Leonardo, H. Löwen, C. Reichhardt, G. Volpe, and G. Volpe, Rev. Mod. Phys. **88**, 045006 (2016).
[3] C. T. MacDonald, J. H. Gibbs, and A. C. Pipkin, Biopolymers **6**, 1 (1968).
[4] C. T. MacDonald and J. H. Gibbs, Biopolymers **7**, 707 (1969).
[5] B. Derrida, Phys. Rep. **301**, 65 (1998).
[6] B. Derrida, E. Domany, and D. Mukamel, J. Stat. Phys. **69**, 667 (1992).
[7] B. Derrida, M. R. Evans, V. Hakim, and V. Pasquier, J. Phys. A: Math. Gen. **26**, 1493 (1993).
[8] B. Derrida, S. A. Janowsky, J. L. Lebowitz, and E. R. Speer, J. Stat. Phys. **73**, 813 (1993).
[9] G. Schütz, Phys. Rev. E **47**, 4265 (1993).
[10] S. Sandow, Phys. Rev. E **50**, 2660 (1994).
[11] B. Schmittmann and R. K. P. Zia, *Statistical Mechanics of Driven Diffusive System*, Phase Transitions and Critical Phenomena Vol. 17, edited by C. Domb and J. Lebowitz (Academic Press, London, 1995).
[12] G. M. Schütz, J. Stat. Phys. **88**, 427 (1997).
[13] G. M. Schütz, *Exactly Solvable Models for Many-Body Systems Far from Equilibrium*, Phase Transitions and Critical Phenomena Vol. 19, edited by C. Domb and J. Lebowitz (Academic Press, London, 2001).
[14] R. A. Blythe and M. R. Evans, J. Phys. A: Math. Theor. **40**, R333 (2007).
[15] M. Kardar, G. Parisi, and Y.-C. Zhang, Phys. Rev. Lett. **56**, 889 (1986).
[16] T. Halpin-Healy and Y.-C. Zhang, Phys. Rep. **254**, 215 (1995).
[17] M. Schliwa, (ed.), *Molecular Motors* (Wiley-VCH, New York, 2003).
[18] K. Svoboda and S. M. Block, Cell **77**, 773 (1994).
[19] M. Schliwa and G. Woehlke, Nature (London) **422**, 759 (2003).
[20] G. Cappello, P. Pierobon, C. Symonds, L. Busoni, J. C. M. Gebhardt, M. Rief, and J. Prost, Proc. Natl. Acad. Sci. USA **104**, 15328 (2007).
[21] P. Reimann, Phys. Rep. **361**, 57 (2002).
[22] I. Raška, K. Koberna, J. Malínský, H. Fidlerová, and M. Mašata, Biol. Cell **96**, 579 (2004).
[23] U. Scheer, B. Xia, H. Merkert, and D. Weisenberger, Chromosoma **105**, 470 (1997).
[24] F. Jülicher and J. Prost, Phys. Rev. Lett. **78**, 4510 (1997).
[25] O. Campàs, Y. Kafri, K. B. Zeldovich, J. Casademunt, and J.-F. Joanny, Phys. Rev. Lett. **97**, 038101 (2006).
[26] N. J. Carter and R. A. Cross, Nature (London) **435**, 308 (2005).
[27] F. Jülicher and J. Prost, Phys. Rev. Lett. **75**, 2618 (1995).
[28] A. B. Kolomeisky and B. Widom, J. Stat. Phys. **93**, 633 (1998).

[29] M. Badoual, F. Jülicher, and J. Prost, Proc. Natl. Acad. Sci. USA **99**, 6696 (2002).
[30] S. Klumpp and R. Lipowsky, J. Stat. Phys. **113**, 233 (2003).
[31] C. Maes and M. H. van Wieren, J. Stat. Phys. **112**, 329 (2003).
[32] A. W. C. Lau, D. Lacoste, and K. Mallick, Phys. Rev. Lett. **99**, 158102 (2007).
[33] R. K. Das and A. B. Kolomeisky, Phys. Rev. E **77**, 061912 (2008).
[34] T. Tripathi and D. Chowdhury, Phys. Rev. E **77**, 011921 (2008).
[35] P. Greulich, A. Garai, K. Nishinari, A. Schadschneider, and D. Chowdhury, Phys. Rev. E **75**, 041905 (2007).
[36] A. Basu and D. Chowdhury, Phys. Rev. E **75**, 021902 (2007).
[37] F. Slanina, Europhys. Lett. **84**, 50009 (2008).
[38] F. Slanina, J. Stat. Phys. **135**, 935 (2009).
[39] F. Slanina, Phys. Rev. E **80**, 061135 (2009).
[40] T. M. Squires and S. R. Quake, Rev. Mod. Phys. **77**, 977 (2005).
[41] G. M. Whitesides, Nature (London) **442**, 368 (2006).
[42] F. Slanina, Phys. Rev. E **94**, 042610 (2016).
[43] F. Slanina, Phys. Rev. E **99**, 012604 (2019).
[44] P. Sajeesh and A. K. Sen, Microfluid. Nanofluid. **17**, 1 (2014).
[45] J. Xuan and M. L. Lee, Anal. Methods **6**, 27 (2014).
[46] T. Salafi, K. K. Zeming, and Y. Zhang, Lab Chip **17**, 11 (2017).
[47] D. Di Carlo, D. Irimia, R. G. Tompkins, and M. Toner, Proc. Natl. Acad. Sci. USA **104**, 18892 (2007).
[48] J. Seo, M. H. Lean, and A. Kole, Appl. Phys. Lett. **91**, 033901 (2007).
[49] A. A. S. Bhagat, H. Bow, H. W. Hou, S. J. Tan, J. Han, and C. T. Lim, Med. Biol. Eng. Comput. **48**, 999 (2010).
[50] D. Di Carlo, Lab Chip **9**, 3038 (2009).
[51] L. R. Huang, E. C. Cox, R. H. Austin, and J. C. Sturm, Science **304**, 987 (2004).
[52] Y. Viero, Q. He, M. Fouet, and A. Bancaud, Electrophoresis **34**, 3300 (2013).
[53] C.-F. Chou, O. Bakajin, S. W. P. Turner, T. A. J. Duke, S. S. Chan, E. C. Cox, H. G. Craighead, and R. H. Austin, Proc. Natl. Acad. Sci. USA **96**, 13762 (1999).
[54] P. K. Ghosh, P. Hänggi, F. Marchesoni, S. Martens, F. Nori, L. Schimansky-Geier, and G. Schmid, Phys. Rev. E **85**, 011101 (2012).
[55] C. Marquet, A. Buguin, L. Talini, and P. Silberzan, Phys. Rev. Lett. **88**, 168301 (2002).
[56] S. Matthias and F. Müller, Nature (London) **424**, 53 (2003).
[57] K. Mathwig, F. Müller, and U. Gösele, New J. Phys. **13**, 033038 (2011).
[58] S. Verleger, A. Grimm, C. Kreuter, H. M. Tan, J. A. van Kan, A. Erbe, E. Scheer, and J. R. C. van der Maarel, Lab Chip **12**, 1238 (2012).
[59] C. Schwemmer, S. Fringes, U. Duerig, Y. K. Ryu, and A. W. Knoll, Phys. Rev. Lett. **121**, 104102 (2018).
[60] C. Kettner, P. Reimann, P. Hänggi, and F. Müller, Phys. Rev. E **61**, 312 (2000).
[61] R. L. C. Cisne Jr., T. F. Vasconcelos, E. J. R. Parteli, and J. S. Andrade Jr., Microfluid. Nanofluid. **10**, 543 (2011).
[62] X. Yang, C. Liu, Y. Li, F. Marchesoni, P. Hänggi, and H. P. Zhang, Proc. Natl. Acad. Sci. USA **114**, 9564 (2017).
[63] M. P. Howard, A. Gautam, A. Z. Panagiotopoulos, and A. Nikoubashman, Phys. Rev. Fluids **1**, 044203 (2016).
[64] S. Solórzano, N. A. M. Araújo, and H. J. Herrmann, Phys. Rev. E **96**, 032901 (2017).
[65] R. Eichhorn, P. Reimann, and P. Hänggi, Phys. Rev. Lett. **88**, 190601 (2002).
[66] R. Eichhorn, P. Reimann, and P. Hänggi, Phys. Rev. E **66**, 066132 (2002).
[67] R. Eichhorn, P. Reimann, and P. Hänggi, Physica A **325**, 101 (2003).
[68] C. Arita, J. Stat. Mech. (2006) P12008.
[69] P. A. Ferrari and J. B. Martin, Ann. Probab. **35**, 807 (2007).
[70] M. R. Evans, P. A. Ferrari, and K. Mallick, J. Stat. Phys. **135**, 217 (2009).
[71] A. Ayyer, J. L. Lebowitz, and E. R. Speer, J. Stat. Phys. **135**, 1009 (2009).
[72] C. Arita and K. Mallick, J. Phys. A: Math. Theor. **46**, 085002 (2013).
[73] N. Crampe, M. R. Evans, K. Mallick, E. Ragoucy, and M. Vanicat, J. Phys. A: Math. Theor. **49**, 475001 (2016).
[74] L. Cantini, A. Garbali, J. de Gier, and M. Wheeler, J. Phys. A: Math. Theor. **49**, 444002 (2016).
[75] N. Crampe, C. Finn, E. Ragoucy, and M. Vanicat, J. Phys. A: Math. Theor. **49**, 375201 (2016).
[76] S. Corteel and L. K. Williams, Sel. Math. New Ser. **24**, 2275 (2018).
[77] A. Ayyer, C. Finn, and D. Roy, Phys. Rev. E **97**, 012151 (2018).
[78] C. Kipnis, C. Landim, and S. Olla, Commun. Pure Appl. Math. **47**, 1475 (1994).
[79] T. Becker, K. Nelissen, B. Cleuren, B. Partoens, and C. Van den Broeck, Phys. Rev. Lett. **111**, 110601 (2013).
[80] C. Arita, P. L. Krapivsky, and K. Mallick, Phys. Rev. E **90**, 052108 (2014).
[81] T. Becker, K. Nelissen, B. Cleuren, B. Partoens, and C. Van den Broeck, Phys. Rev. E **93**, 046101 (2016).
[82] C. Arita, P. L. Krapivsky, and K. Mallick, Phys. Rev. E **94**, 016101 (2016).
[83] C. Arita, P. L. Krapivsky, and K. Mallick, Phys. Rev. E **95**, 032121 (2017).
[84] C. Cocozza-Thivent, Z. Wahrscheinlichkeitstheorie Verw. Geb. **70**, 509 (1985).
[85] T. Seppäläinen, Ann. Probab. **27**, 361 (1999).
[86] G. M. Schütz, J. Phys. A: Math. Gen. **36**, R339 (2003).
[87] V. Popkov, J. Schmidt, and G. M. Schütz, Phys. Rev. Lett. **112**, 200602 (2014).
[88] V. Popkov, J. Schmidt, and G. M. Schütz, J. Stat. Phys. **160**, 835 (2015).
[89] S. Ghosh, T. Bameta, D. Ghanti, and D. Chowdhury, J. Stat. Mech. (2016) 123501.
[90] F. C. Alcaraz and R. Z. Bariev, Phys. Rev. E **60**, 79 (1999).
[91] G. M. Schütz, R. Ramaswamy, and M. Barma, J. Phys. A: Math. Gen. **29**, 837 (1996).
[92] M. R. Evans and T. Hanney, J. Phys. A: Math. Gen. **38**, R195 (2005).
[93] If we have proportion $\frac{a}{b} = \frac{A}{B}$ whose value is ϕ, then $\frac{A+\nu a}{B+\nu b} = \phi$, where ν is an arbitrary number. This is obtained by adding νab to both sides of $aB = Ab$.